Western University
Scholarship@Western

Masters of Clinical Anatomy Projects

Anatomy and Cell Biology Department

Spring 4-30-2015

PHENOTYPIC ANALYSIS OF LONG BONES IN PANNEXIN 3 KNOCKOUT MICE

Deidre Caskenette
dcaskene@uwo.ca

Follow this and additional works at: https://ir.lib.uwo.ca/mcap

Part of the Anatomy Commons

PHENOTYPIC ANALYSIS OF LONG BONES IN PANNEXIN 3 KNOCKOUT MICE
USING A GEOMETRIC MORPHOMETRIC APPROACH

BY

DEIDRE CASKENETTE

GRADUATE PROGRAM IN CLINICAL HUMAN ANATOMY

A THESIS SUBMITTED IN PARTIAL FULFILLMENT
OF THE REQUIREMENTS FOR THE DEGREE OF
MASTER OF SCIENCE

THE SCHOOL OF GRADUATE AND POSTDOCTORAL STUDIES
THE UNIVERSITY OF WESTERN ONTARIO
LONDON, ONTARIO, CANADA

Abstract

Pannexin 3 (Panx3) is a channel forming glycoprotein that is highly expressed in skeletal tissues. Panx3 is induced at the growth plate of long bones where it regulates cell proliferation and differentiation, a key role in bone formation.

This study analyzes the phenotype of long bones in a novel Panx3 knockout (KO) mouse to assess the role of Panx3 in bone formation.

Ten KO and 10 wild-type (WT) adult mice were scanned using in vivo micro-CT. Right femora / humeri were digitized using homologous landmarks. Geometric morphometric analysis (multivariate statistical methods) allowed for quantitative comparison of shape, size and variation between KO and WT long bones.

KO mice demonstrated distinct long bone shape differences. A significant amount of this difference, 20-30%, can be attributed to the allometric component of shape. When scaled, WT bones have proportionally longer diaphyses and KO bones have larger bony prominences and epiphyses.

Analysis of long bone cross-sectional geometric properties revealed thicker diaphyses in KO mice, equaling greater resistance to torsion and compression.

KO mice appear to have altered long bone growth patterns, implicating a role for Panx3 in maintaining optimum skeletal growth.

Keywords

Acknowledgments

I would like to thank the people without whom this project would not have been possible. Thank-you to all members of my advisory committee who were always patient in working out scheduling conflicts, generous with their time and dedicated to providing honest counsel. Your expertise and openness to new ideas have been invaluable.

I thank the team at Robarts Research Institute, who patiently aided me in developing the skills to extract and interpret the images that enabled the gathering of our data. For your pervading logic and willingness to attend to all my queries, I am ever grateful.

It is with special thanks that I acknowledge Drs. Laird and Penuela for including me as part of their team and without whom the Pannexin 3 knockout mouse line and the CT scans used in this project would not have been available. For all their tangible contributions, and for their candid and sound advice as I navigated the world of pannexin biology, I offer my sincere appreciation. Dr. Laird reminded me to always relate our findings to the greater significance and to build a story from those findings to make them relevant and accessible to our audience; for this wise counsel, I thank you. Dr. Penuela, for your expertise and grounded advice, but also for your ever patient and gracious approach to teaching this sometimes labored learner, I thank you.

Last, but certainly not least, I express my utmost respect and heartfelt gratitude to my supervisor, Dr. Katherine Willmore, whose energy, enthusiasm and optimism know no bounds. Tireless and persistent in the face of every obstacle and false start, you passionately guided and encouraged me in testing new realms. You inspired faith that we could persuade the far-flung pieces of this project to coalesce and form a relevant work. It is my hope that we have accomplished in these pages, a unified and meaningful story, worthy of the telling.

Table of Contents

List of Tables

List of Figures

1   Background

Communication amongst cells is essential for normal function and development in an organism. To accomplish adequate communication, cells use channels that span the membranes of adjacent cells, known as gap junctions, and single-membrane channels connecting intracellular and extracellular regions. In chordates, gap junctions and hemichannels (half of a cell to cell channel) are formed by a family of proteins knows as connexins. Invertebrate cells use an unrelated, but topologically similar family of proteins known as innexins to form gap junctions.

In the search for innexin homologues in chordates, a new class of pore forming proteins now known as pannexins were identified in 2000 (Panchin et al. 2000). Pannexins are a class of transmembrane glycoproteins found in chordates that have limited sequence homology with innexins (Panchin et al. 2000). Although pannexins were initially thought to function in a similar manner to innexins, forming gap junctions for intercellular communication, the majority of evidence now indicates that pannexin proteins function to form single-membrane channels connecting the intracellular and extracellular compartments (Penuela et al. 2007; Sosinsky et al. 2011; Penuela, Gehi, and Laird 2013). These channels facilitate the movement of ions and small molecules resulting in the induction of multiple signaling pathways; current evidence has identified pannexins as ATP release channels (Bao, Locovei, and Dahl 2004; Ishikawa et al. 2011) initiating signaling cascades (Scemes, Spray, and Meda 2008; Penuela et al. 2014; Ishikawa et al. 2011).

There are three members of the pannexin protein family, Panx1, Panx2 and Panx3. The role of each pannexin in cellular processes continues to be discovered, but most cell types express at least one of the pannexins (Bond and Naus 2014).

1.1　　Pannexin Structure

All members of the pannexin family have 4 transmembrane domains, 2 extracellular loops, 1 intracellular loop, and cytoplasmic terminal domains (Baranova et al. 2004) (Figure 1). The three pannexins vary in their amino acid lengths; Panx2 is the largest and all members contain two cysteine residues in each extracellular loop and undergo glycosylation at specific sites (Penuela, Gehi, and Laird 2013) (Figure 1). Panx1 and Panx3 each exist in three forms that are dependent upon their glycosylation. Different forms are localized to particular parts of the cell and glycosylation also appears important for Panx1 and Panx3 to properly reach the cell surface (Boassa et al. 2007; Penuela et al. 2007). Panx1 is known to associate with several proteins; Panx1 was shown to interact with actin at its C-terminal tail as well as to form an association with several other proteins that appear to control gating and cell trafficking (Bond and Naus 2014).
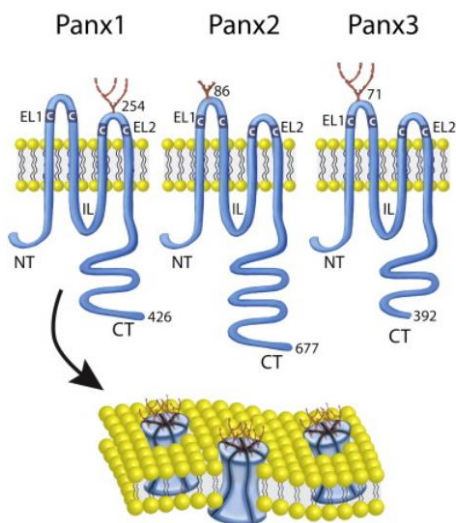
Biochimica et biophysica acta. Biomembranes by ELSEVIER BV. Reproduced with permission of ELSEVIER BV in the format Thesis/Dissertation (Penuela, Gehi, and Laird 2013)

Figure 1. Diagram depicting the three pannexins. Each member differs in amino acid length with Panx2 being the largest. All members have 4 transmembrane domains, 2 extracellular loops (EL1, EL2), 1 intracellular loop (IL), and cytoplasmic terminal domains, CT (carboxy-terminus) and NT (amino-terminus). All have specific sites of glycosolation and two cysteine residues (C) in each extracelluar loop. Subunits oligomerize to form channels.

Pannexin subunits oligomerize to form channels called pannexons (Figure 1). Panx1 oligomerizes into hexameric structures to form a channel, while Panx2 forms heptamers or octamers. Oligomerization data for Panx3 is still outstanding, although it is predicted to also form hexamers since it has a similar polypeptide sequence and size as Panx1 (Penuela, Gehi, and Laird 2013).

Members of the pannexin family have been reported to interact to form intermixed channels: Panx1 with Panx2 or Panx1 with Panx3 (Bruzzone et al. 2005; Bond and Naus 2014; Penuela et al. 2009). There appears to be no change in function associated with mixing of Panx1 with Panx3, although the Panx1/2 configuration results in diminished function of the channel (Bruzzone et al. 2005; Penuela et al. 2009) and is unstable when isolated (Ambrosi et al. 2010). This intermixing of pannexins along with evidence of phenotypes that can be observed only in double knockout pannexin mice suggests that members of the pannexin family may compensate for each other when one is absent or insufficient. In this respect, it is also notable that Panx2 and Panx3 are often co-expressed in tissues with Panx1 (Penuela et al. 2009).

1.2   Expression of Pannexins

All three pannexins have been identified in various chordate species including humans, mice, rats, dogs, cows, zebrafish, and puffer fish (Yen and Saier Jr 2007). Notably, human pannexins have up to 94% conserved sequence homologies with murine pannexins (Penuela et al. 2009).

Pannexins have been characterized in a number of human and murine tissues. Panx1 is the most extensively studied of the pannexin family and has the most widespread tissue distribution; it has been identified in brain, heart, skeletal muscle, skin, testis, ovary,

placenta, thymus, prostate, lung, liver, small intestine, pancreas, spleen, colon, endothelium, and erythrocytes (Baranova et al. 2004). Panx1 has also been detected in chondrocytes and in osteoblasts (Penuela, Gehi, and Laird 2013; Bond and Naus 2014; Moon et al. 2015). Panx2 expression is limited mainly to areas of the brain (Bruzzone et al. 2003; Baranova et al. 2004).

Of the three pannexins, Panx3 is the least studied and has the most limited expression profile. It is largely expressed in skeletal tissues and skin (Baranova et al. 2004; Penuela et al. 2007; Bond et al. 2011; Ishikawa et al. 2011), but has also been found in arterioles within the kidneys (Bond and Naus 2014) and in Leydig cells, the epididymis and efferent ducts of adult rats (Turmel et al. 2011). Recently, there is also evidence of Panx3 in skeletal muscle tissues (Langlois et al. 2014).

1.3　　The Role of Pannexins in Physiology, Development and Disease

In recent years, pannexins have been the subject of intense investigation as their roles in physiology and disease continue to be uncovered. As outlined above, one or more of the pannexins are expressed in most mammalian tissues, indicating a potential link to many physiological and pathological processes. For example, Panx1 has been found to be involved in a diverse range of processes including vasodilation, vasoconstriction, taste sensation, viral infection, immune response, tumor suppression in gliomas vs tumor proliferation in melanomas, stroke, epilepsy, and regulation of keratinocytes in the skin (Penuela et al. 2014; Celetti et al. 2010; Cowan et al. 2012).

Panx2 has been found to have a role in neuronal differentiation and is reduced in gliomas (Lai, Bechberger, and Naus 2009). As well, Panx2 has been linked to ischaemia / stroke (Penuela et al. 2014).

The only disease process linked to Panx3 thus far is osteoarthritis. Panx3 is upregulated in osteoarthritic cartilage, and knocking out the protein in cartilage has a protective effect against the development of osteoarthritis (Moon et al. 2015). In vitro studies have identified important roles for Panx3 in bone growth and development (Ishikawa et al. 2014; Ishikawa et al. 2011; Iwamoto et al. 2010). These processes and the current understanding of Panx3's role in formation and maintenance of the skeleton are discussed below.

1.4 Exploring the Role of Panx3 in Bone Growth and Development

In vitro studies to date have demonstrated that Panx3 is highly expressed in skeletal tissues. It is present in the developing growth plate of long bones, and is induced during the differentiation of chondrocytes (Iwamoto et al. 2010). Panx3 is also expressed in osteoblasts and promotes their differentiation (Ishikawa et al. 2011). Owing to the induction of Panx3 at the growth plate of developing long bones demonstrated in-vitro, it is expected that in-vivo, a lack of Panx3 will effect an observable phenotype related to long bones. To further explore the role of Panx3, a summary of long bone development by endochondral ossification is first provided, followed by a summary of our current knowledge of the role of Panx3 in the growth and development of long bones. Finally, our study and how it aims to further elucidate the role of Panx3 in bone formation is introduced.

1.5   Overview of Long Bone Growth and Development

In mammals, bones form by one of two distinct processes during embryonic development. Intramembranous ossification is the process by which many of the craniofacial bones develop directly from condensations of mesenchymal cells. However, the long bones of mammals develop by a process of endochondral ossification whereby a precursor model made of hyaline cartilage first forms and is then replaced by bone. Endochondral ossification also enables longitudinal growth and healing of long bones (Ross and Pawlina 2011) .

The transition from cartilage to bone is dependent on controlled chondrocyte and osteoblast differentiation. There are numerous molecules involved in an array of pathways that regulate the differentiation and behavior of these cells.

The process of endochondral ossification begins with the aggregation of mesenchymal stem cells. Although all the molecular mechanisms required for this clustering of mesenchymal cells are not entirely understood, there are a number of elements involved in the process including adhesion molecules, the transcription factor SOX9, Hox proteins, fibroblast growth factors (FGFs) and bone morphogenic proteins (BMPs) (Long and Ornitz 2013) . Cells in the center of the aggregate differentiate into chondrocytes while those at the periphery form the perichondrium (Long and Ornitz 2013).

Differentiation of chondrocytes is regulated by FGFs, and the transcription factors, SOX9, SOX5, and SOX6. As well, BMPs induce the differentiation of mesenchymal cells through SMAD protein signaling pathways (Long and Ornitz 2013). Chondrocytes secrete cartilage matrix (in hyaline cartilage the main matrix components are type II

collagen, glycosaminoglycans, proteoglycans and glycoproteins). Through the action of these components, the cartilaginous model of the bone is (Ross and Pawlina 2011).

Chondrocytes proliferate and continue to secrete matrix resulting in growth of the cartilage model. Chondrocytes in the center mature, stop proliferating and hypertrophy. The hypertrophy of the chondrocytes is associated with secretion of type X collagen, matrix calcification, vascular invasion, and chondrocyte death followed by resorption of the calcified matrix and replacement by bone. The hypertrophied chondrocytes release alkaline phosphatase, an enzyme that is required for mineralization of the cartilage matrix (Fedde et al. 1999; Anderson 1969). Hypertrophic chondrocytes secrete vesicles containing phosphates into columns of the matrix between rows of chondrocytes such that longitudinal septae are well calcified serving as scaffold for future bone deposition; the poorly calcified transverse partitions allow for subsequent infiltration of blood vessels (Amizuka et al. 2012).   Chondrocytes, now surrounded in calcified matrix, are restricted from nutrients and die. This death results in breakdown of much of the matrix resulting in formation of a cavity. Concurrently, cells of the perichondrium in the mid region of the cartilage model differentiate into osteoblasts that secrete bone matrix resulting in formation of a bony collar in the diaphyseal region of the developing bone. As well, vascular endothelial growth factor (VEGF) is released at the time of hypertrophy which attracts blood vessels into the center of the cartilage mold. The invasion of blood vessels brings osteoprogenitor cells which differentiate into osteoblasts and deposit bone matrix (osteoid) onto calcified cartilage spicules left behind by the death of the chondrocytes. In this way, trabecular bone is produced. Resorption of the calcified matrix driven by the appearance of proteolytic enzymes, most notably MMP13, and replacement with trabecular bone is stimulated. This initial site of bone formation in the center of the long bone is known as the primary ossification center (Ross and Pawlina 2011). The cartilage matrix continues to be resorbed and haematopoietic stem cells arrive to form the marrow.

Between the newly generated bone and the cartilage of the epiphysis, the primary growth plate develops. Here, the maturing chondrocytes are arranged in distinctive zones. Furthest from the primary ossification center and nearest the epiphysis is the zone of resting chondrocytes. Moving toward the center of the diaphysis, the zones of proliferative, maturing, and hypertrophic chondrocytes are evident (White and Wallis 2001; Ross and Pawlina 2011). Zones of calcified cartilage and resorption can also be identified toward the center of the diaphysis.

In the resting zone, chondrocytes do not appear to proliferate or secrete matrix and probably serve as precursors for the proliferating chondrocytes in the adjacent, zone of proliferation (Kronenberg 2003). In the proliferative zone, chondrocytes divide, align in distinct columns, and secrete matrix constituents including collagen (mainly type II). Some studies identify a pre-hypertrophic zone, where chondrocytes enlarge and are in the process of maturing. Next to the pre-hypertrophic zone is the zone of hypertrophy, where chondrocytes are greatly enlarged. The hypertrophic chondrocytes remain active in secreting collagen (now increasingly type X) as well as VEGF and alkaline phosphatase. In the zone of calcified cartilage, the matrix becomes calcified and the hypertrophied chondrocytes begin to die. The zone of resorption is nearest the center of the diaphysis and is free of chondrocytes. Here, blood vessels invade and calcified cartilage forms spicules that serve as scaffold for the arriving osteoblasts to deposit new bone (Ross and Pawlina 2011).

Secondary centers of ossification develop at proximal and distal ends of the bone (epiphyses) soon after birth. These ossification centers develop by the same process as the primary center whereby chondrocytes hypertrophy and degenerate, the matrix calcifies and blood vessels invade bringing osteogenic cells. In growing long bones, proliferating chondrocytes remain in the regions between each epiphysis and diaphysis (between the primary and secondary ossification centers) in the form of transverse cartilaginous discs known as the growth plates. The bone lengthens as the chondrocytes

in the growth plates proliferate and secrete matrix, pushing the epiphysis further from the diaphysis. The cartilage is replaced by bone during growth by the same mechanism as during development. During growth, there is a balance between proliferation and resorption such that the thickness of the growth plate remains consistent. In humans, the growth plates fuse at puberty and longitudinal growth ceases at this time. Radial growth is achieved through bone deposition by the cells of the periosteum. Although longitudinal growth ceases at puberty, bone remodeling continues throughout life.

These processes of growth and remodeling, like development, are tightly controlled by both local and systemic factors. Systemic factors include growth hormone, estrogen, vitamin D, glucocorticoids and thyroid hormone. Locally produced factors include hedgehog proteins, FGFs, Wnts and BMPs (Kronenberg 2003) . Recent years have seen progress in understanding the role and interactions of these local factors in regulating bone growth and differentiation.

1.6   Signaling Molecules Regulating Bone Growth

1.6.1   Indian hedgehog and parathyroid hormone-related peptide regulate chondrocyte proliferation and differentiation

Indian hedgehog (Ihh) is a signaling factor that is secreted by pre-hypertrophic and hypertrophic chondrocytes. Binding to its receptor, Patched-1 (Ptc) triggers a cascade leading to stimulation of chondrocyte proliferation. Ihh also indirectly inhibits chondrocytes from entering the hypertrophy stage by inducing the expression of parathyroid hormone-related peptide (PTHrP) (St-Jacques, Hammerschmidt, and McMahon 1999; Mackie et al. 2008).

PTHrp is a protein secreted by cells of the perichondrium and early proliferative chondrocytes; its receptor (the same G-protein-coupled receptor used by parathyroid hormone) is expressed at high levels by chondrocytes in the pre-hypertrophic zone. Ihh binding to its receptor induces the production of PTHrP; binding of PTHrP to its receptor then delays chondrocyte hypertrophy through cAMP dependent signaling. Once cells have gone through hypertrophy they stop producing Ihh. PTHrP and Ihh form a negative feedback loop regulating chondrocyte entry into hypertrophy.

Ihh is also necessary for differentiation of mesenchymal cells into osteoblasts for formation of the bony collar prior to formation of the primary ossification center and for osteoblast differentiation in both perichondrial cells and in the formation of trabecular bone. In the absence of Ihh, perichondrial cells fail to express the transcription factor Runx2, which is necessary for osteoblast differentiation (Long and Ornitz 2013).

1.6.2 Fibroblastic growth factor (FGF) regulates chondrocyte proliferation and differentiation

There are 22 distinct genes encoding the structurally related FGF family of proteins and four genes encoding their receptors. FGF proteins and receptors are expressed at every level of endochondral ossification where they are involved in regulating chondrocyte proliferation and differentiation (Ornitz and Marie 2002). The fibroblast growth factor receptor-3 (FGFR3) is the best understood. Activation of this receptor inhibits chondrocyte proliferation and promotes hypertrophic differentiation of chondrocytes independent of other signaling systems (Minina et al. 2002). However, FGFR3 also exerts this effect by decreasing the expression of Ihh. Therefore, FGFR3 shortens the zone of proliferating chondrocytes by decreasing chondrocyte proliferation and by suppressing Ihh expression (Minina et al. 2002; Kronenberg 2003).

1.6.3 Bone morphogenetic protein (BMP) Signaling

BMPs are another family of signaling molecules that are expressed at all stages of endochondral ossification. They are known to oppose the action of FGF in that they enhance the expression of Ihh and increase chondrocyte proliferation (Naski et al., 1998; Minina et al., 2002; Yoon et al., 2006). These antagonistic signaling systems demonstrate the importance of balancing interacting elements for proper bone development. BMP signaling is also important in promoting osteoblast differentiation and functioning.

1.6.4 Transcription Factors: SOX9 and Runx2

SOX9 is a transcription factor essential for chondrogenesis. It is expressed in the cells of mesenchymal condensations and in proliferating chondrocytes, but not in hypertrophic chondrocytes. Without SOX9, mesenchymal cells do not differentiate into chondrocytes and there is absence of cartilage and bone formation (Akiyama et al. 2002; Bi et al. 1999). When Sox9 is deleted at later stages, most cells remain as mesenchymal condensations and do not differentiate into chondrocytes; there is also decreased expression of molecules of the Ihh-PTHrP pathways. As well, SOX9 is needed for expression of SOX5 and SOX6, other related transcription factors that act together with SOX9 for appropriate proliferation and timing of chondrocyte hypertrophy (Akiyama et al. 2002; Smits et al. 2004). Together the SOX transcription factors activate genes for components of the extracellular matrix and allow differentiation of progenitor cells into chondrocytes (de Crombrugghe et al. 2000; Long and Ornitz 2013; Smits et al. 2001).

The transcription factor Runx2 has important roles in the growth plate where, along with Runx3 it promotes differentiation of chondrocytes from proliferative to hypertrophic and stimulates expression of Ihh (Yoshida et al. 2004). As well, it is required for osteoblast

formation and function (Otto et al. 1997; Komori et al. 1997). Panx3 expression also appears to be regulated by Runx2 activity (Bond et al. 2011) .

1.6.5   Wnt family of Proteins

Members of the Wnt family of proteins are signaling molecules involved in the regulation of many biological processes (Alberts 2008). Wnts can activate three types of intracellular signaling pathways. One of these pathways, known as the canonical Wnt signaling pathway, is important in bone formation as it promotes osteoprogenitor proliferation and regulates bone mass (Glass et al. 2005). This pathway is dependent on the gene regulatory protein, B-catenin (Alberts 2008).

In the absence of Wnt, B-catenin binds to a degradation complex that includes the scaffold protein, Axin, glycogen synthase kinase (GSK) and casein kinase 1 (CK1); once bound, B-catenin is phosphorylated by CK1 and GSK which leads to B-catenin degradation (Alberts 2008) . When Wnt binds to a frizzled receptor, and the lipoprotein receptor-related protein (LRP) co-receptor, the scaffold protein, Dishevelled and Axin are recruited to the plasma membrane. The degradation protein complex is disrupted resulting in inhibition of B-catenin phosphorylation. Therefore, in the presence of Wnt, B-catenin accumulates in the cytoplasm and is then translocated to the nucleus. Here, it binds to transcription factors that activate transcription of proteins required for cell cycle progression as occurs in the proliferation stage of osteoprogenitor cells (Glass et al. 2005; Behrens et al. 1996; Alberts 2008).

Protein kinase A (PKA), which is dependent on intracellular cAMP levels, positively regulates the Wnt pathway by phosphorylating and inactivating GSK, resulting in inhibition of B-catenin degradation (Fang et al. 2000; Suzuki et al. 2008). As well, PKA

activates the cAMP-response element-binding (CREB) family of transcription factors which activates expression of genes for proliferation (Behrens et al. 1996).

The PTHrP/PTH signaling pathway has a role in regulation of the Wnt pathway in that PTHrP/PTH binding to their receptor activates G proteins, which, in turn activate adenylyl cyclase to generate cAMP from ATP. Increased cAMP levels then increase activity of PKA. Subsequent activation of CREB then induces genes required for proliferation (in both chondrocyte and osteogenic cells) (Iwamoto et al. 2010).

1.6.6   Role of Panx3 in Long Bone Growth and Development

The current understanding of the role of Panx3 in bone biology is limited to in-vitro, and ex-vivo studies. It has been shown in these studies that Panx3 plays an important role in skeletal development as it promotes the switch from proliferation to differentiation in chondrocytes and osteoprogenitor cells (Iwamoto et al. 2010; Ishikawa et al. 2014). Evidence to date indicates that Panx3 has its effect on these processes by forming a channel that promotes the release of ATP into the extracellular space and by action as an ER calcium channel that allows for increased intracellular calcium (Iwamoto et al. 2010; Ishikawa et al. 2011; Ishikawa et al. 2014).

1.6.7   Role of Panx3 in Chondrocyte Regulation

As outlined above, endochondral ossification, the process by which long bones are formed, requires a skeletal template of cartilage. In the developing growth plate, chondrocytes organize into discrete zones according to their stage of maturation. Chondrocyte proliferation and differentiation must be spatially and temporally controlled

by the activity of numerous molecules and signaling systems for the formation of a healthy skeleton. Panx3 is implicated as one such molecule with an important role in the regulation of these processes.

In endochondral ossification, Panx3 is first expressed by chondrocytes in the prehypertrophic zone of the developing growth plate (Iwamoto et al. 2010; Ishikawa et al. 2011). Here, it forms channels that allow release of ATP from the interior of the cell to the extracellular space. Research has shown that this ATP release may lead to inhibition of the PTH/PTHrP signaling pathway that drives chondrocyte proliferation (Iwamoto et al. 2010).

It is surmised that the Panx3 induced release of ATP out of the cell reduces intracellular cAMP levels, thus inhibiting PKA/CREB signaling which has the effect of down-regulating proliferation. Panx3 expression also promotes the differentiation of chondrocytes from a proliferative to post-mitotic state (Iwamoto et al. 2010).

1.6.8   Role of Panx3 in Osteoblast Regulation

Panx3 is also expressed in osteoprogenitor cells and osteoblasts (Iwamoto et al. 2010; Ishikawa et al. 2011). Panx3 is induced during differentiation of osteogenic cells. Osteoblast marker genes are up-regulated and mineralization increased in cells over-expressing Panx3 and these aspects of bone development are down-regulated in Panx3 inhibited cells, indicating a role for Panx3 in promoting differentiation of osteoblasts (Ishikawa et al. 2011).

Calcium is known to be involved in many signaling pathways, including the calcium-calmodulin system that promotes osteoblast differentiation (Zayzafoon, Fulzele, and McDonald 2005; Seo et al. 2009). Panx3 was localized to the plasma membrane and was co-localized with a marker of the endoplasmic reticulum (ER), an organelle that stores calcium, suggesting Panx3 is localized in the ER (Ishikawa et al. 2011). Panx3 over-expressing osteoprogenitor cells that were stimulated by ATP demonstrated increased intracellular calcium levels. As well, Panx3 transfected cells showed increased activity of calcium-calmodulin and increased levels of downstream proteins in this pathway (Ishikawa et al. 2011).

Panx3 expression reduced intracellular ATP and increased extracellular ATP. Extracellular ATP can bind to purinergic receptors that initiate signaling pathways that activate ER calcium channels. Evidence suggests that the Panx3 ER calcium channel is activated when this purinergic binding activates the P13K-Akt pathway, a mechanism distinct from that of other ER calcium channels. (Ishikawa et al. 2011).

Calcium binding to calmodulin can then activate molecules downstream that promote osteoblast differentiation (Seo et al. 2009). Increased calcium also initiates signaling cascades that promote degradation of p53, an inhibitor of differentiation (Ishikawa et al. 2011) and that increase protein levels and activation of p21, a protein that promotes cell cycle exit (Ishikawa et al. 2014). Thus, Panx3 promotes osteoblast differentiation by functioning as a plasma membrane channel releasing ATP and by acting as an ER channel that increases intracellular calcium signaling.

Some signaling pathways important in osteoprogenitor proliferation and differentiation have been identified. However, understanding regarding the regulation of these signaling pathways and the mechanism by which osteoprogenitors transition from proliferation to differentiation remains incomplete. Panx3 appears to have a key role in this transition by

inhibiting osteoprogenitor proliferation and promoting cell cycle exit through several signaling pathways (Ishikawa et al. 2014).

Osteoprogenitor proliferation and bone mineralization are promoted by the canonical Wnt signaling pathway (Glass et al. 2005; Kato et al. 2002; Ishikawa et al. 2014). It has been shown that Panx3 expression inhibits osteoprogenitor proliferation and promotes cell cycle exit (Ishikawa et al. 2014). Exogenous Wnt has the effect of increased cell proliferation in normal osteoprogenitor cells. However, proliferation is inhibited in Panx3 over-expressing cells despite the addition of exogenous Wnt. Localization of B-catenin to the nucleus is decreased and phosphorylation of B-catenin is increased in Panx3 over-expressing cells whereas phosphorylation of GSK3 is inhibited (Ishikawa et al. 2014).

Panx3 is induced by BMP prior to mineralization (Bond et al. 2011; Ishikawa et al. 2014). Panx3 channels promote release of ATP from the cell to the extracellular space; this movement of ATP initiates multiple Panx3 signaling pathways that act to inhibit proliferation of osteoprogenitor cells and to promote cell cycle exit (Ishikawa et al. 2014). Release of ATP decreases the amount of cAMP that can be produced in the cell. PKA, when activated by cAMP, functions to phosphorylate and inhibit GSK3. As cAMP is reduced upon Panx3 expression, the action of PKA is reduced and GSK3 activity is increased. Therefore, B-catenin is phosphorylated and degraded and there is reduced transcription of genes necessary for proliferation.

2   INTRODUCTION

2.1   Pannexin 3 and Long Bone Biology

Taken together, current evidence supports the involvement of Panx3 in multiple signaling pathways required for appropriate skeletal development and growth. These pathways are induced when Panx3 single membrane channels promote release of ATP from the cell to the extracellular space. The increased extracellular ATP has the effect of activating purinergic receptors initiating the P13K-Akt pathway and other purinergic regulated pathways for ER calcium release leading to subsequent activation by calcium of signaling cascades that promote cell cycle exit and promote differentiation. As well, ATP release reduces intracellular cAMP levels leading to inhibitory regulation of Wnt and PKA-CREB pathways required for cell proliferation. Therefore, Panx3 plays an important role in bone formation by inhibiting cell proliferation and promoting chondrocyte and osteoblast differentiation; these regulatory processes are required for bone growth and mineralization.

2.2   Shape Differences

To examine the morphology of the long bones of Panx3 KO mice and compare the phenotype to that of WT mice, a quantitative shape analysis approach was used. This quantitative approach to shape comparison is a branch of statistics known as geometric morphometrics. It describes a set of methods used to analyze landmark coordinate data using multivariate statistics.   A landmark is a point in two or three-dimensional space corresponding to a feature of interest on an object (Zelditch, Swiderski, and Sheets 2012). Landmark analysis is always multivariate in that a shape is described by a configuration of landmarks and cannot be described by a single point.

The benefits of using landmark coordinate data when performing shape comparisons include preserving information about spatial relationships between points and preserving the original geometries of the forms. Therefore, landmarks allow us to elucidate information about the nature and location of differences. Landmark analysis also allows for easy visualization and communication of shape differences among complex forms while still providing a quantitative and precise description. It allows for statistical analysis of the average form as well as variation about the average (Frelat et al. 2012). Landmark data are also superior in detecting subtle or complex shape differences that can be common when comparing specimens of the same species (Baab, McNulty, and Rohlf 2012). Another strength of landmark data analysis is that it allows for a separation of shape variation from total size variation and allows for investigation of the relationship between size and shape (Baab, McNulty, and Rohlf 2012). A limitation of this type of landmark coordinate data is that it does not describe the curvatures of a form. It is also not always possible to find evenly spaced landmarks, so that there may be more landmarks in one area of a form than in another.

By examining the localized shape differences between long bones of KO vs WT mice, it may be possible to identify those areas most affected by Panx3 and therefore identify those processes most affected. Findings may direct future investigation into as yet unknown mechanisms regulating normal and pathological bone development.

2.3   Cross-Sectional Geometry

Long bone shape and size reflect not only their genetic and developmental history, but also reflect adaptations to their mechanical environment over time (Lieberman, Polk, and Demes 2004). The cross-sectional geometric properties of a long bone are aspects of structural variation that can be used to predict the mechanical performance of the bone under applied forces and assess "loading history" or mechanical adaptations of the bone

(Lieberman, Polk, and Demes 2004). This type of analysis has been useful in fields such as orthopaedics where mechanical performance is of great clinical significance (Burstein and Wright 1994) and in anthropological research where it has allowed for inferences about the behavior and lifestyle of extant populations based on skeletal remains (Katzenberg and Saunders 2008).

These applications are possible due to the propensity of living skeletal tissues to respond to application of mechanical forces by way of adaptations that influence their morphology. This premise that mechanical loading of bone results in structural changes of the bone is often referred to as "Wolff's Law", named after the 19th century orthopaedic surgeon who popularized the concept. However, in its original form, Wolff intended to formulate strict mathematical rules to describe the process and the concept may better be described today as "bone functional adaptation" to mechanical loading (Katzenberg and Saunders 2008; C. Ruff, Holt, and Trinkaus 2006).

Bone functional adaptation can most simply be described by a feedback model of bone adaptation where bone deposition / resorption is stimulated based on maintaining an "optimum customary level" of strain. Strain is the physical deformation of the bone tissue under force and as strain increases, such as when activity levels increase, there is net bone deposition thereby restoring the original amount of strain. When strain decreases beyond a set-point, bone is resorbed to restore original levels (Katzenberg and Saunders 2008; Sumner-Smith and Bishop 1982; C. Ruff, Holt, and Trinkaus 2006). The "customary level" of strain, however, can vary according to skeletal location and systemic factors such as age, disease, diet, hormonal factors and genetics (Katzenberg and Saunders 2008; Lieberman, Devlin, and Pearson 2001; C. Ruff, Holt, and Trinkaus 2006; Pearson and Lieberman 2004). The frequency and type of strain, and loading history of the bone are other variables that influence the response of bone to its mechanical environment (Burr, Robling, and Turner 2002; C. Ruff, Holt, and Trinkaus 2006).

Support for this optimum strain model of functional adaptation come from animal studies (Burr, Robling, and Turner 2002; Robling et al. 2002; Woo et al. 1981; C. Ruff, Holt, and Trinkaus 2006) that demonstrate the response of bone to loading is to preferentially increase deposition of bone in areas of greatest strain. As well, improved resistance in exercised bone appears to have little to do with bone mineral density or the quality of bone, which changes little, but can instead be attributed to increases in the quantity and distribution of bone; these characteristics are represented by the geometric properties of the bone (Burr, Robling, and Turner 2002; Robling et al. 2002; C. Ruff, Holt, and Trinkaus 2006; Woo et al. 1981).

The engineering concept of beam theory whereby properties of strength and rigidity of a beam can be calculated given the geometrical properties of the structure can be applied to a long bone. A long bone diaphysis can be considered as behaving like a hollow beam when mechanical loads are applied (Huiskes 1982; Katzenberg and Saunders 2008; C. B. Ruff and Hayes 1983).In beam theory, "strength" refers to the maximum amount of stress (force per unit area) a structure can sustain prior to failure; (Reilly and Burstein 1974). "Rigidity" is a measure of a structure's resistance to deformation under externally applied forces. Strength can be thought of as a structure's ability to resist breaking and rigidity as a structure's ability to remain stiff and resist bending (Katzenberg and Saunders 2008).

Different types of mechanical stresses can affect a beam structure. Axial compression and tension act along the long axis to compress or stretch the material respectively. Bending creates compressive and tensile forces on opposite sides of a cross-section; torsion refers to twisting about the long axis which produces shearing (diagonal) forces (Katzenberg and Saunders 2008).

Cross-sectional geometric properties of a bone can be used to quantify the strength and rigidity of a bone in relation to these different kinds of mechanical loadings. Cross-

sectional area of a beam reflects the beam's resistance to pure compression and tension (loads applied along the long axis which is perpendicular to the cross-section); in a long bone, the cross-sectional area is equal to the cortical area, denoted, CA. However due to the curvature of bones and the direction of muscle pull, among other factors, bones are rarely subjected to purely axial loads. Most often, bones are subjected to bending and torsion that describe bending about a particular axis (C. B. Ruff and Hayes 1983; Katzenberg and Saunders 2008). These more relevant mechanical loadings are proportional to cross-sectional geometric properties known as second moments of area.

Second moments of area are the product of unit areas of material and the squared distances of these areas to the axis in the plane of bending (units are mm^4). Therefore, both the total area of material and its distribution about a defined axis are included in this measure. Second moments of area can be calculated about any axis through the section depending on the direction of the applied bending force and are designated, I, with a subscript indicating the axis about which they were calculated. They are usually calculated about anatomical axes (mediolateral and anteroposterior) or as maximum and minimum (I_{max} and I_{min}). I_{max} and I_{min} are always orthogonal to each other and indicate the magnitudes of the greatest and least bending rigidities of the section respectively.

Second moments of area calculated about the central point (centroid) of the section or the sum of any two perpendicular measures of I (eg. $I_{max} + I_{min}$), are known as polar second moments of area, designated, J, and describe the structure's resistance to torsion as well as the average bending rigidity. Therefore, J is the most important cross-sectional geometric property for describing a bone's overall rigidity (C. B. Ruff and Hayes 1983; Lieberman, Polk, and Demes 2004).

Upon application of bending or torsional forces, maximum stress occurs at the outermost surface of the cross-section. Therefore, bone tissue that is distributed further from the

centroid will provide more resistance to bending and torsional forces (Bertram and Swartz 1991). To provide an index of "strength", second moments of area are divided by the distance from the outermost surface to the neutral axis (0 strain) for bending or to the centroid for torsion. This property is referred to as section modulus, Z.

However, in the absence of experimental strain data, J has proven the most accurate estimate of a bone's average bending rigidity (Lieberman, Polk, and Demes 2004). Z compounds errors associated with deviation of bending axes from the centroid in-vivo due to unpredictable factors such as changes in ground surface, limb positioning, and muscle forces involved (Lieberman, Polk, and Demes 2004; C. Ruff, Holt, and Trinkaus 2006).

Due to such complexities, calculations of cross-sectional properties from long bone geometry are approximations of in-vivo bone rigidity and strength and there is considerable error (30-50%) involved regarding absolute values (Lieberman, Polk, and Demes 2004; C. Ruff, Holt, and Trinkaus 2006). However, these calculations remain valid indicators of mechanical performance when used for comparison of relative in-vivo properties for the same bone within a species or between similar species where loading patterns are similar (Lieberman, Polk, and Demes 2004; C. Ruff, Holt, and Trinkaus 2006).

2.3.1   Bone Shape

The mechanical performance of a bone is a function of both the amount of tissue and the distribution of that tissue. Therefore, not only do the size and mass of a bone contribute to its rigidity, so does its shape determine these properties. In anthropological studies of fossilized remains, it is theorized that differences in the massiveness of long bone

diaphyses between populations reflect varying levels of activity whereas differences in shape reflect alternate patterns of activity (Trinkaus et al. 1991). Support for this theory comes from animal studies (Carlson and Judex 2007; Nunamaker, Butterweck, and Provost 1990) and studies of human athletes (Shaw and Stock 2009a; Shaw and Stock 2009b; Macdonald, Cooper, and McKay 2008) that demonstrate changes in diaphyseal shape that reflect adaptation to specific mechanical loading patterns and overall increases in cortical bone related to increased activity levels.

Quantification of diaphyseal cross-sectional shape for use in comparisons is accomplished using I_{max}/I_{min}. This ratio estimates the distribution of cortical bone relative to the centroid. I_{max} and I_{min} are a function of the distribution of tissue in the section and therefore provide a better measure of shape than any other ratio of second moments of area (Shaw and Stock 2009b). It is also of note that this ratio can be used to judge the reliability of J as an accurate indicator of rigidity. As the section departs from circularity, the reliability of J as an index of rigidity decreases (Daegling 2002; Shaw and Stock 2009b).

2.3.2   Other Cross-Sectional Properties

Other values obtained from analysis of cross-sectional geometry are useful as descriptors of a bone's morphology. The total subperiosteal area, denoted TA, is the total area within the bone's perimeter and the medullary area is denoted MA and it is the area of the medullary canal. These qualities also describe the relative distribution of bone in a section. The percent cortical area calculated CA/TA X 100 is another descriptor of cortical thickness and the relationship of tissues in the section (Katzenberg and Saunders 2008).

2.4   Objectives and Rationale

Despite the crucial role that Panx3 plays in bone development, there are no overt phenotypic effects of knocking out Panx3 in a mouse model (Moon et al. 2015). While the role of Panx3 in bone development has been studied in cultured cells, it has not been systematically explored in vivo. Additionally, the apparent contradiction between the key role of Panx3 in bone development, and the lack of gross phenotypic effects upon ablation of the protein remains unexplained. To begin to address the paucity of understanding in these areas, and help uncover the role of Panx3 in physiological processes, a novel Panx3 knockout (KO) mouse line was used. This mouse globally lacks Panx3 in all tissues.

In this study, the phenotypic aspects of long bones in KO and WT mice were compared to further elucidate the role of Panx3 in bone formation. Specifically, the study quantifies and compares the shape, size, bone mineral density and cross-sectional geometric properties of the femur and humerus between KO and WT mice.

2.5   Hypothesis

It is hypothesized that Panx3 KO mice will demonstrate differences in long bone shape (greatest at the growth plates), with decreased size, decreased bone mineral density, and indexes of decreased mechanical performance when compared to WT controls. As well, greater variability is expected in KO than WT mice.

3   METHODS

3.1   Animals

The sample consisted of 10 adult wildtype and 10 adult Panx3 knockout mice. Panx3 KO
mice were obtained that had been generated using embryonic cells with a C57BL/6N
origin and using the Cre/IoxP recombinase system (Moon et al. 2015). WT mice were
C57BL/6 non-littermate controls.

All mice were male and were 2 or 3 months of age at the time of scanning. Two KO mice
and 4 WT mice were 3 months old at the time of scanning and all other mice were 2
months of age. At the time of scanning, the average weight of WT mice was 26.3 grams
and the average weight of KO mice was 24.6 grams. There was no significant difference
in weight between the two groups at the time of scanning (p = 0.14; Figure 8).

3.2   Micro-computed Tomography Imaging

High resolution micro-computed tomography (μCT) whole body images of the mice were
obtained using the eXplore speCZT μCT scanner (GE Healthcare, Waukesha, WI, USA)
at Robarts Research Institute (London, ON, Canada). Mice were anesthetized through
face-cone administered isofluorane (Forane, catalog #CA2L9100, Baxter Corporation,
Mississauga, ON Canada) and imaged using in-vivo scanning techniques following
Granton and colleagues (2010). In one rotation of the beam, 900 views were obtained at
0.40 intervals over a 5 minute period (16ms exposure). Images were acquired at isotropic
voxel size of 50 μm and reconstructed into 3D volumes at 100 μm to reduce noise
associated with breathing. Two separate scans were required to capture the whole mouse.

The two scans were later digitally 'stitched' together to render a full 3D volume of the entire mouse. Total scan time per animal was 10 minutes. Calibration samples of water and a synthetic cortical-bone mimicking epoxy with a bone mineral equivalent of 1,100 mg/cm3 (SB3, Gamex, Middleton, WI, USA) were imaged in a separate scan to ensure accurate calibration of CT greyscale intensities in Hounsfield Units (HU).

3.3   Segmentation

Reconstructed images were then examined using MicroView. Right femora and humeri were isolated from the whole body images by manually segmenting each bone using MicroView.

3.4   Landmark-Based Data Collection and Analyses Methods

3.4.1   Choosing Landmarks

When choosing landmarks, criteria of homology, adequate coverage and repeatability were considered. Three-dimensional coordinates were recorded for each specimen (Figure 2; Figure 3).For biological and mathematical purposes, the most important criterion is that of homology (Zelditch, Swiderski, and Sheets 2012). Here, the term homologous refers to choosing landmarks as discrete points that can be recognized as the same anatomical loci on all specimens (Zelditch, Swiderski, and Sheets 2012). The position of each 3-dimensional landmark is then recorded as a set of x-, y-, and z-coordinates.

As much as possible, landmarks were also chosen to provide adequate coverage of the form. However, it is noted that landmarks could not be chosen over the articulating joint surfaces as manual segmentation of the bones from their joint did not allow for a clean outline of these surfaces. Landmark repeatability was tested empirically by performing repeat measurements and discarding those landmarks that were not reliably repeatable.

3.4.2   Landmark Acquisition

The software package, etips (a multidimensional volume visualization and analysis software co-developed by the NIH and the National University of Singapore) was used to reconstruct surface representations of the segmented right femur and right humerus from each mouse. Landmarks were then taken from these reconstructions. To determine suitability of landmarks, for the femora and then the humeri, 4 bones were digitized 4 times. Points that could be repeated within 0.05mm of error were deemed acceptable (Frelat et al. 2012).

3.4.3   Femur Sample

Fourteen, three-dimensional landmarks were collected from the right femur of each mouse in the study (n=18). Femora from two mice (one WT and one KO) were not used due to movement artifacts that prevented accurate landmark collection. Each femur was digitized twice and the averaged coordinate data were used for subsequent analyses. All data were screened for outliers.

Table 1. List of Femoral Landmarks (Figure 2) Used in this Study and their Anatomical Description.

Femoral Landmarks		
Landmark Number	Landmark Identifier	Description of Landmark Location
1	in	Intercondylar fossa
2	gts	Tip of greater trochanter
3	gtp	Tip of third trochanter
4	ditc	Distal intertrochanteric crest
5	pitf	Point of greatest curvature of longest arm of third trochanter
6	gtl	Anterior corner of greater trochanter
7	ptt	Proximal end of third trochanter
8	dtt	Distal end of third trochanter
9	ltsd	Distal end under lesser trochanter on shaft
10	tgta	Line where third trochanter meets greater trochanter
11	lep	Lateral epicondyle
12	lps	Lateral aspect of superior tip of patellar articular surface
13	mps	Medial aspect of superior tip of patellar articular surface
14	mep	Medial epicondyle
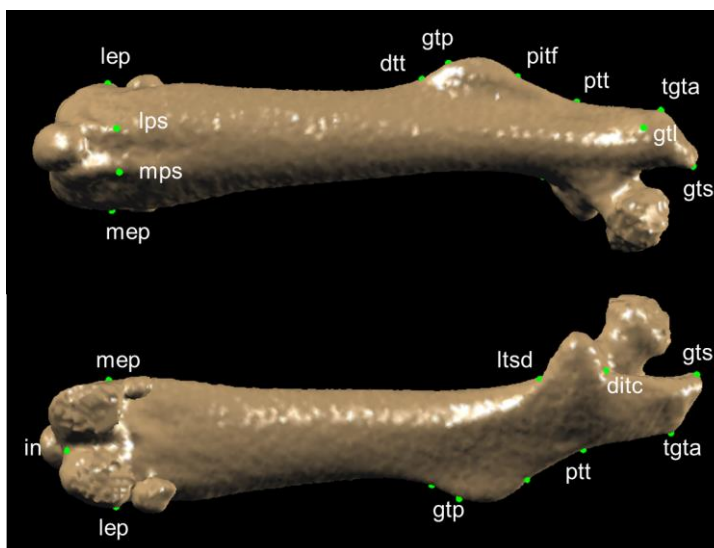
Figure 2. Mouse femur in rostral view (above) and caudal view (below) with the 14 landmarks used in this study superimposed.

3.4.4   Humerus Sample

The right humerus from each mouse (n=20) was digitized twice using 12, three-dimensional landmarks. The average coordinates for each landmark were used for analysis. All data were screened for outliers.

Table 2. List of Humeral Landmarks (see Figure 3) Used in this Study and their Anatomical Description.

Humeral Landmarks		
Landmark Number	Landmark Identifier	Description of Landmark Location
1	ins	Superior point on proximal growth plate in between greater and lesser tubercle
2	pgp	Superior point on proximal growth plate lateral view
3	mltgp	Medial side greater tubercle meets proximal growth plate
4	lgtgp	Lateral side tubercle meets growth plate
5	hlt	Between head of humerus and lesser tubercle at level of growth plate
6	pdt	Proximal deltoid tuberosity
7	tdt	Tip of deltoid tuberosity
8	ddt	Distal deltoid tuberosity
9	lep	Lateral epicondyle
10	sc	Supinator crest (most lateral point)
11	cf	Olecranon fossa
12	mep	Medial epicondyle
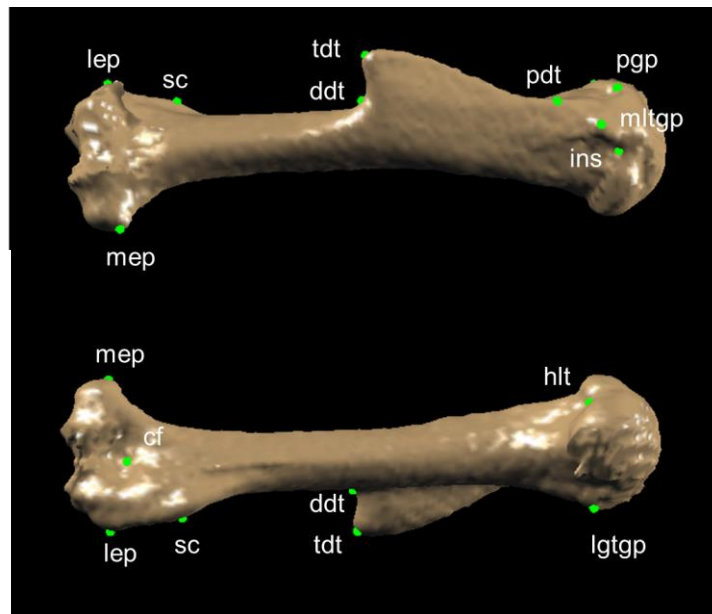
Figure 3. Mouse humerus in rostral view (above) and caudal view (below) with the 12 landmarks used in this study superimposed.

3.5   Analysis

3.5.1   Shape and Size

In analysis of landmark data for this study, principal components analysis (PCA) was first used to investigate and visualize patterns in the data. Euclidean Distance Matrix Analysis (EDMA) (Lele and Richtsmeier 2001) was then used to quantify and localize differences. Investigation for differences in variances of interlandmark distances was statistically evaluated with a bootstrap approach using MIBoot (Cole, 2002).

3.5.2   PCA

To simplify the description of variation in the sample and allow for better visualization and interpretation of the distribution of that variation in a small sample size, PCA was used. All bones included in the study as defined by 14 landmarks (femur) or 12 landmarks (humerus) were superimposed by means of a general Procrustes analysis whereby landmark configurations are translated, rotated and scaled so as to minimize the squared distances between corresponding landmarks (Rohlf and Slice 1990). The resulting Procrustes coordinates were analyzed by PCA.

PCA finds the axes of greatest variation in the dataset; principal component 1 (PC1) is the line through the data that accounts for the largest amount of variation, and each successive axis is orthogonal to previous axes and explains a successively smaller proportion of the variation (Richtsmeier et al. 1998; Zelditch, Swiderski, and Sheets 2012). Most of the variation is explained in the first two principal components, thereby reducing the number of variables that need be viewed. A score is determined for each

individual of the sample that represents its distance from the mean of the sample. These principal component scores allow each individual to be plotted on the principal coordinate axes. The relative positions of the data points remain the same and we can see how individuals group relative to each other and in terms of the axes that describe most of the variation in the sample.

This type of analysis is appropriate for statistical comparisons with smaller sample sizes where there are many variables and few specimens, as reducing the number of variables that need be considered allows us to increase the statistical power and detect meaningful differences (Zelditch, Swiderski, and Sheets 2012). PCA analysis on Procrustes coordinates allows for comparison of the overall shape and size of the long bones while maintaining the relative geometry of landmarks (Zelditch, Swiderski, and Sheets 2012) (For a more in depth discussion of PCA, see Appendix A).

3.5.3   Euclidean Distance Matrix Analysis (EDMA)

While PCA is useful for simplifying and describing the variation in an overall form, it is also beneficial to consider localized shape differences. As well, Procrustes based analysis assumes a normal distribution of variance, limiting its use with a small sample size in analyses other than PCA.

Another approach, Euclidean Distance Matrix Analysis (EDMA), is a non-parametric landmark analysis method that allows for statistically consistent results even with a small sample of specimens (Richtsmeier et al. 1998). EDMA also allows visualization of how differences are localized. In this analysis, comparison of aspects of form and shape does not depend on an arbitrary choice of a common coordinate system or on the variance about a point. Therefore, the aspects considered in the comparison do not vary with

translation, rotation or reflection of the object (Lele and Richtsmeier 2001). This approach is based on distances between landmark pairs and quantifies differences using matrix algebra (Lele and Richtsmeier 2001).

Therefore, landmark data was further analyzed using EDMA. To accomplish this analysis, the landmark coordinates were used to calculate all possible linear distances (Euclidean distances) between landmark pairs. A matrix consisting of these distances is known as the form matrix (FM) and represents the individual specimen. An average FM is then determined for each group. The average form matrix from each group is compared and the difference between forms is expressed as a form difference matrix (FDM). Elements of the FDM correspond to the ratios (division of an element in one form matrix by its corresponding element in the other form matrix) of the linear distances.

To account for size differences, the geometric mean of all distances can be used as a scaling factor to create a shape matrix (Lele and Richtsmeier 2001). The outcome is size-corrected forms that, when compared, are considered a comparison of shape. The mean shape difference matrix represents the shape difference between sample groups. The elements of the shape difference matrix correspond to the difference between like linear distances of the two shape matrices. For a more in-depth discussion of EDMA, see Appendix B.

3.5.4 Use of Confidence Intervals for Statistical Comparison of Localized Differences

The estimated form difference matrix can determine if a particular distance is larger in one group than in the other. To determine if the difference in the interlandmark distance is statistically significant, confidence intervals are used (Lele 1995; Lele and Richtsmeier

2001). To obtain the confidence intervals, a Bootstrap approach is used. This approach involves random sampling with replacement. The bootstrap simulates what might happen if the experiment were repeated many times over with more individuals. A random sample of the landmark coordinate matrices representing individuals is taken from each group with replacement. The mean form difference matrix is then calculated for the samples obtained. These steps are repeated 1000 times.

As introduced by Lele and Richtsmeier (1995), a confidence interval is obtained for each interlandmark distance by sorting the obtained ratios. If the interval between the upper and lower confidence limits contains the value 1, then it is likely that this particular distance is not different in the two groups when comparing form. (When comparing shape, if the interval contains the value 0 then the distances are likely not different). The interval also provides an idea as to the magnitude of the difference between groups for a particular distance. This type of analysis is appropriate for small sample sizes as it removes the sample size constraints of parametric statistics.

3.5.5   Shape Variance

To compare the differences in variances of interlandmark distances between groups, and to statistically evaluate these differences using a bootstrap approach, the Windows-based software package, MIBoot was used (Cole 2002).

3.6 Bone Mineral Density (BMD)

MicroView software (GE Healthcare Biosciences) was used to calculate bone mineral density (BMD) where BMD is the ratio of the average HU value of the bone region under examination to the measured HU value of the SB3 calibrator (Beaucage et al. 2014). The difference in BMD between groups was tested for significance using a Welch's two-sample t-test and a Wilcoxon rank sum test in R statistical computing environment.

3.7 Cross-Sectional Geometric Properties

3.7.1 Data Collection

Segmented bones were aligned in MicroView and 100 micron slice thickness cross-sections obtained orthogonal to the long axis of each bone. Due to movement artifact, two WT and two KO mice were excluded from cross-sectional geometric analyses. Diaphyseal cross-sectional locations were determined based on percentages of bone length. Cross-sections were obtained at 50% of bone length for the femur and at 40% of bone length measured from the distal end for the humerus (to avoid the deltoid tuberosity). Similar cross-sectional locations have been used in previous studies assessing long bone diaphyseal mechanical performance (Ruff 2002).

The cross-sectional scans were then imported into the ImageJ (NIH) and a consistent density threshold to represent bone was set. MomentMacro, a plugin for ImageJ was used to calculate cortical bone area (CA), total subperiosteal area (TA), second moments of area (I_{max}, I_{min}) and second polar moment of area (J). Obtained values were used for further calculations of I_{max}/I_{min}, and percent cortical area (%CA) (see Table 4).Cross-

sectional geometric properties were statistically compared using Welch's t-tests and Wilcoxon rank sum test using R statistical environment. P-values were adjusted for multiple tests using the Bonferroni correction.

3.8 Standardization

When comparing the structural and mechanical properties of bone amongst individuals, body size and limb proportions must be considered as these characteristics influence mechanical loading and skeletal mass. There is the general acceptance that measures of cross-sectional area are best standardized using body mass and that second moments of area are standardized using the product of body mass and bone length (ie moment arm) (Katzenberg and Saunders 2008; Stock and Shaw 2007).

Therefore, to control for any variation in body size, second moments of area (I_{max}, I_{min}) and polar second moments of area (J) were standardized by the product of body mass and bone length^2. Cortical area (CA) and total subperiosteal area (TA) were standardized by body mass. The following standardization formulas were used: J/(Body Mass X Length^2); CA/Body Mass; TA/Body Mass; I_{max}/(Body Mass X Length^2); I_{min}/(Body Mass X Length^2). TA is the total subperiosteal area and %CA is CA/TA X 100.

Full-length bone measurements were performed in MicroView. Femur length was measured as the distance from the most superior point of the greater trochanter to the most inferior point of the distal epiphysis and humerus length was measured from the greater tubercle to the distal epiphysis.

4 RESULTS

4.1 Size and Shape of Long Bones

4.1.1 Principal Components Analysis

Differences between WT and KO mice were compared using Principal Components Analysis (PCA) in MorphoJ. In the PCA analysis, a regression on age was first performed and residuals used for subsequent analysis in order to remove any effect of age on shape.

Femoral and humeral shape as determined by the first two principal components are depicted in scatterplots in Figure 4. Within the femur, PC1 accounts for 40% of the total variance, PC2 accounts for 16% of the variance, and PC3 accounts for 10% of the variance. For the humerus, 57% of the total variance is represented by PC1, 10% is represented by PC2, and 7% of the variance is represented by PC3. Thus, the majority of variance is represented by the first two principal components. This analysis shows that the shape of KO and WT femora and humeri are differentiated along PC1 as shown in Figure 4 (A, B).

Femoral and humeral shape with the allometric component removed as determined by the first two principal components are depicted in scatterplots in Figure 4 (C, D). In the femur, PC1 accounts for 30% of the total variance, PC2 accounts for 18% of the variance and PC3 accounts for 11% of the variance. For the humerus, 40% of the total variance is represented by PC1, 15% by PC2, and 10% by PC3 when the size component of shape is removed. When the allometric component of shape is removed (regression of shape on size), there is no distinct separation of the groups (Figure 4 (C, D)). These groupings

demonstrate that much of the difference between WT and KO bone shape is attributable to a difference in their size proportions.

Performing a regression of shape on size separates the component of variation that is predicted by size from the residual component of variation. Using the residuals from this regression, Morpho J calculates the percentage of total shape variation that is due to size variation. When this analysis is carried out on the femur data, centroid size accounts for 20% of the total shape variance among individuals. Permutation testing against the null hypothesis of independence between shape and size variables was also performed. The null hypothesis was rejected and it is indicated that size accounts for a significant portion of the femoral shape difference between groups ($p < 0.01$).

For the humeri, the allometric component of shape accounts for 30% of the total shape variance among individuals. A permutation test determined that the allometric component of shape accounts for a statistically significant proportion of total shape variation ($p < 0.01$).

Thus, PCA demonstrates that KO femora and humeri shape differs from that of WT mice and that a significant portion of the overall shape difference is due to allometric differences.
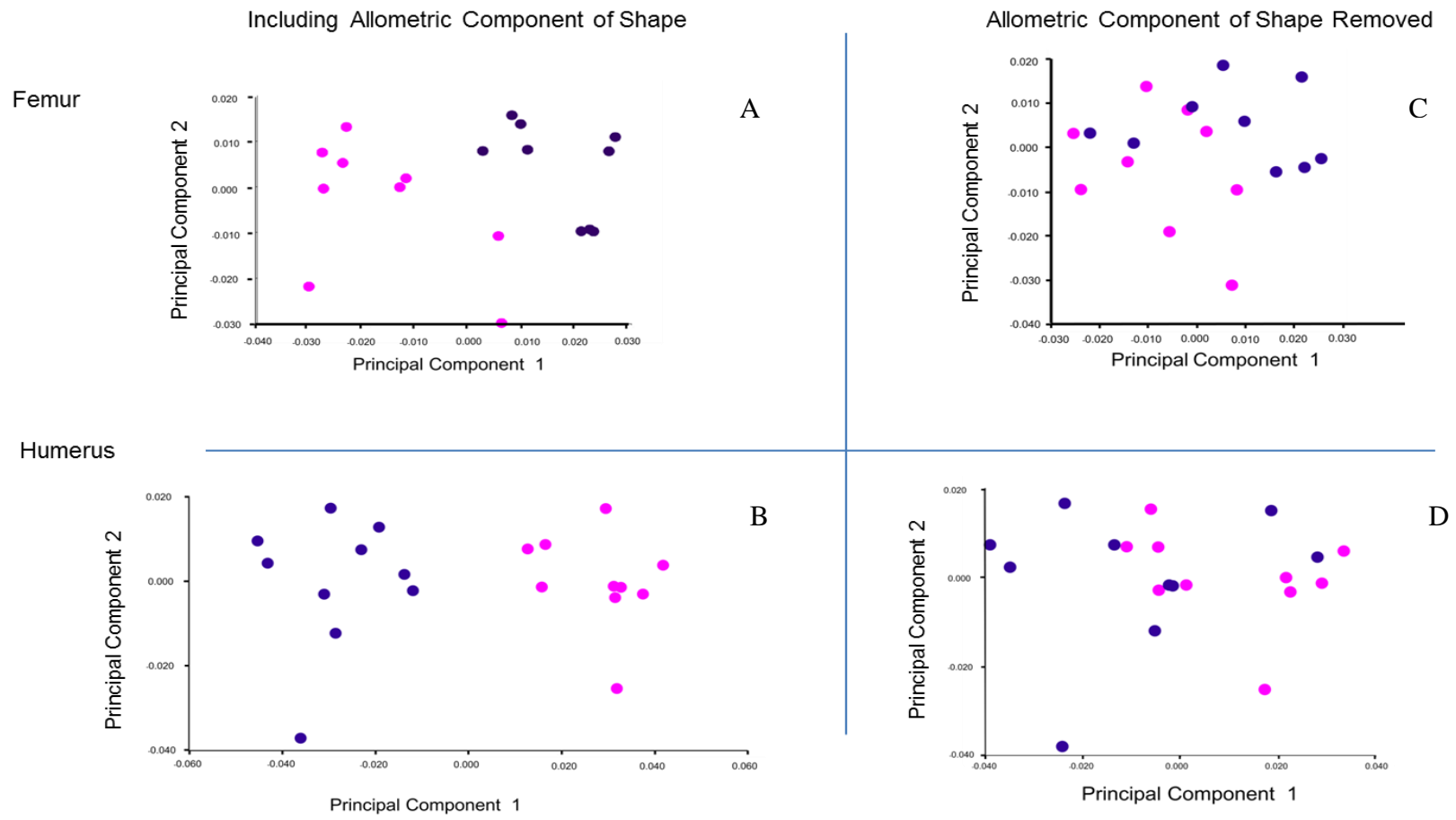
Figure 4. Scatterplots of the first two principal components for the femur and humerus with (A, B) and without (C, D) the allometric component of shape. WT and KO humeral and femoral shape are differentiated along PC1 when the allometric component of shape is included (A, B).

4.1.2   EDMA Analysis

4.1.2.1   Form Difference Results

Form analysis of the femur reveals that 17/91 (19%) distances are larger in KO than in WT. However only 1 of those distances is significantly greater (in – lep). The vast majority of distances, 74/91 (81%), are greater in WT than in KO; 45 of these distances (49%) are significantly greater in WT than in KO mice.

Form analysis of the humerus reveals that 12/66 (18%) distances are greater in KO than in WT. However, none of these distances are significantly greater. The majority of distances, 54/66 (82%), are greater in WT than in KO; 34 of these distances (51%) are significantly greater in WT than in KO mice.
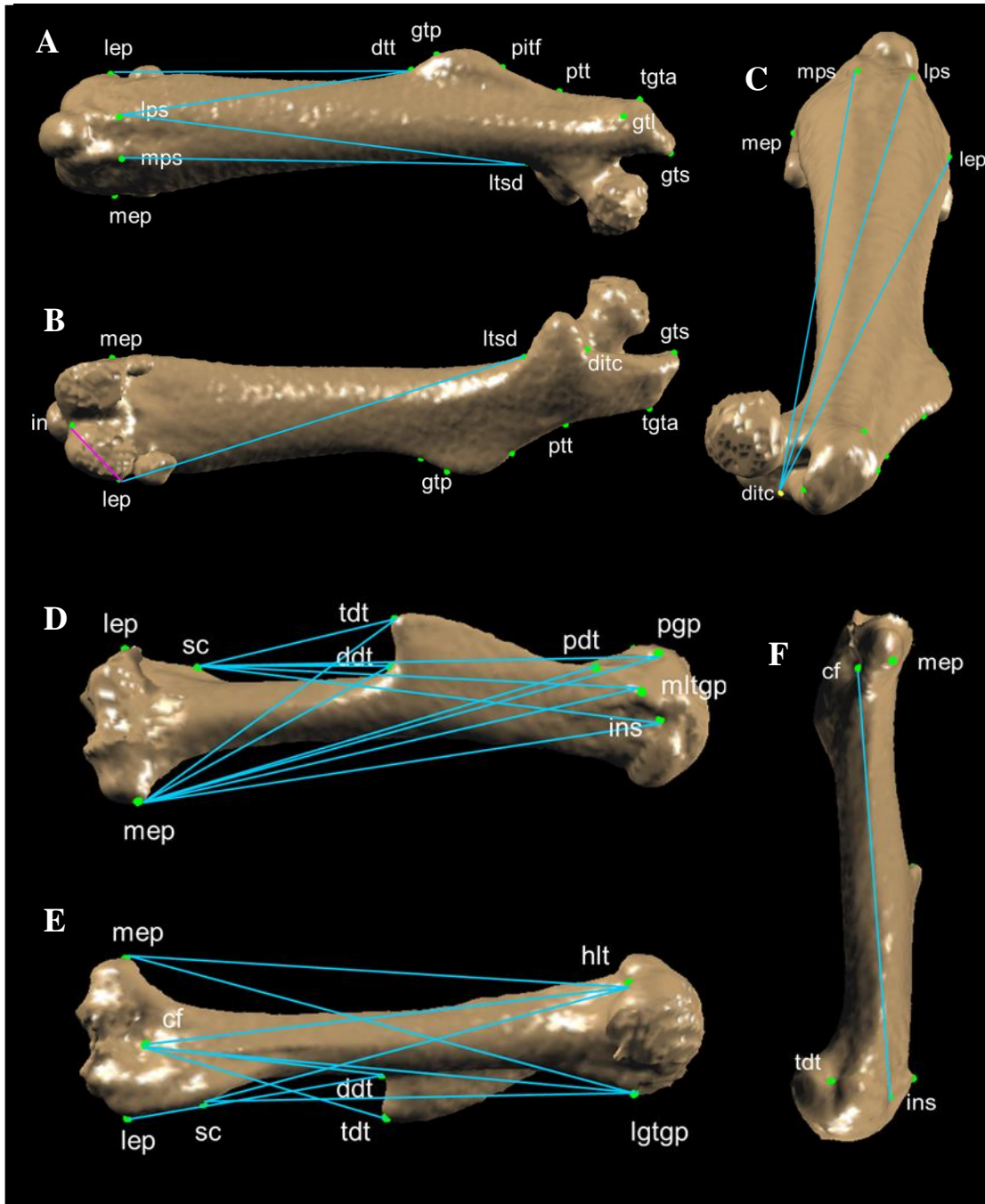
Figure 5. Femoral (A-C) and humeral (D-F) linear distances that are significantly different in form between WT and KO mice as determined by confidence interval testing. Distances that are greater in WT than KO by at least 5% are drawn in blue. The distance that is significantly greater in KO than in WT is drawn in pink. (A) rostral , (B) caudal, (C) supero-rostral views of the mouse right femur. (D) rostro-medial, (E) caudal, (F) supero-medial views of right humerus.

WT greater than KO by intervals of 5-10% to 7-13%

KO greater than WT 1-8%

4.1.2.2   Shape Difference Results

Shape analysis of the femur reveals that 41/91 (45%) distances are larger in KO than in WT. Of those distances, 13 (14%) are significantly greater in KO than in WT mice. Approximately half of the distances, 48/91 (53%), are greater in WT than in KO. Of these distances, 38 (42%) are significantly greater in WT than in KO mice.

Shape analysis of the humerus reveals that 36/66 (54%) distances are greater in KO than in WT; 22 (33%) of the distances are significantly greater in KO than in WT mice. 30/66 (45%) distances are greater in WT than in KO; 25 (38%) of the distances are significantly greater in WT than in KO mice.

Figure 6. Femoral (A-C) and humeral (D-G) linear distances that are significantly different in shape by confidence interval testing and differ by up to 5% or more between WT and KO mice. Distances that are greater in WT than KO mice are drawn in blue, and those that are greater in KO than WT mice are drawn in pink. (A) rostral , (B) caudal, (C) supero-rostral views of the mouse right femur. (D) rostromedial, (E) caudal, (F) medial, (G) lateral views of right humerus.

WT greater than KO by intervals of 5-9% to 6-12%

KO greater than WT by intervals of 1- 5% to 2-6%

4.1.2.3   Shape Variance and Correlations

Based on confidence interval tests calculated in MIBoot, the variance in distances between groups did not differ significantly for femoral or humeral data.

A regression on age for individual distances was performed; those distances that were found to be significantly correlated with age ($p \geq 0.05$) are indicated in Supplementary Tables 5-11; these distances were not included in Results (Figures 5,6).

4.2   Bone Mineral Density and Weight Comparisons

Table 3. Femoral/Humeral Bone Mineral Density and Length and Full Body Weight

Measurement	Summary Statistics						Welch's t-test		Wilcoxon Rank Sum Test	
		WT			**KO**					
	N	Mean	SD	N	Mean	SD	t score	p value	W	p value
Femur BMD (mg/cm^3)	10	14.75	2.81	10	16.77	3.54	1.42	0.17	28	0.11
Humerus BMD (mg/cm^3)	10	14.76	2.41	10	15.41	2.13	0.64	0.53	41	0.53
Weight (g)	10	26.3	2.97	10	24.62	1.58	1.57	0.14	60	0.47
Femur Length (mm)	8	**15.27**	0.48	8	**14.36**	0.33	**4.87**	**0.00017***	**95**	**0.00021***
Humerus Length (mm)	8	**11.56**	0.33	8	**11.18**	0.25	**2.85**	**0.01 ***	**79**	**0.034 ***

Bone mineral density of femora and humeri was slightly greater in KO than WT mice (Figure 7, Table 3). However, this difference is statistically insignificant as calculated using Welch's t-test and Wilcoxon rank sum test (Table 3).

Wildtype mice were slightly heavier than KO mice as depicted in Figure 8 (mean weight: WT 26.3g, KO 24.6g). However, this difference in weight is statistically insignificant as determined by Welch's t-test and Wilcoxon rank sum test (Table 3). All mouse weights are listed in supplementary Table 12.

Bone length was greater in WT mice than in KO mice and this difference is statistically significant as determined by Welch's t-test and Wilcoxon rank sum test (Table 3). All mouse femoral/humeral lengths are listed in supplementary Table 13.
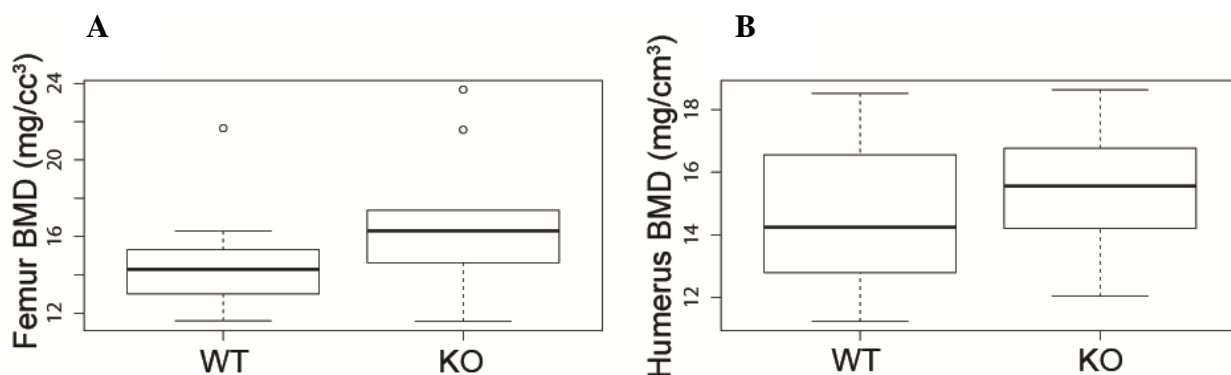
Figure 7. (A) The average bone mineral densities of WT and KO femora were compared. KO femora demonstrated a slightly higher bone mineral density than WT, although the difference was not statistically significant. (B) The average bone mineral densities of WT and KO humeri were compared. KO humeri demonstrated a slightly higher bone mineral density than WT, although the difference was not statistically significant. Boxes represent the 25th-75th percentile range, with the horizontal dark line indicating the median; whiskers extending to the maximum and minimum values within 1.5 box lengths. Outliers are indicated by ○.
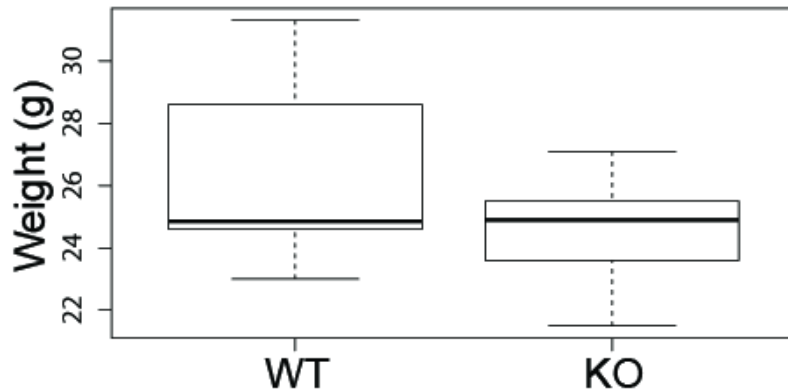
Figure 8. The average weight of the WT and KO groups at the time of scanning were compared. Differences in weight were not statistically significant (Table 3). Boxes represent the 25th-75th percentile range, with the horizontal dark line indicating the median; whiskers extending to the maximum and minimum values within 1.5 box lengths.
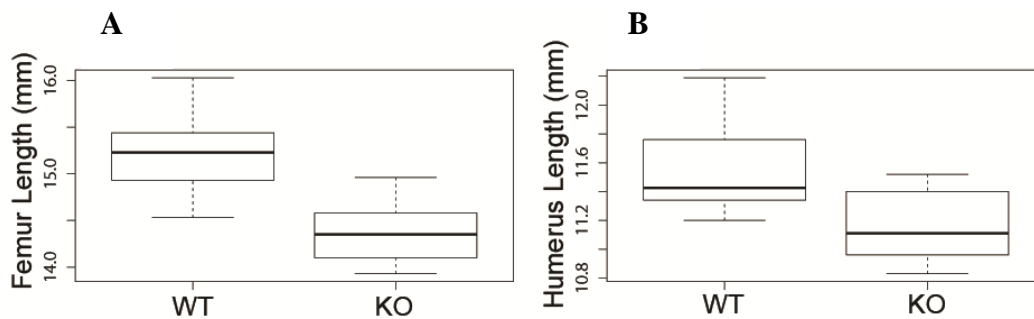
Figure 9. (A) Femur, and (B) Humerus bone lengths were compared between KO and WT mice. WT mice demonstrated significantly longer bone lengths than KO mice (Table 3). Boxes represent the 25th-75th percentile range, with the horizontal dark line indicating the median; whiskers extending to the maximum and minimum values within 1.5 box lengths.

4.3   Cross-Sectional Geometry Analysis

Cross-sectional properties of femora and humeri were compared between WT and KO mice.

After correction for multiple tests using the Bonferroni correction, significant differences were found for the polar second moment of area, J, in both bones and for CA in the femur as determined by Welch's t-test and Wilcoxon rank sum test (Table 4, Figures 10, 11 (A, C)). For all three differences, KO mice had greater measures than WT. Using this conservative measure of significance, CA was not significantly different in the humerus although the trend of greater CA in KO than in WT mice remains. Thus, KO mouse long bones demonstrate greater resistance to torsion (J) and compression (CA). Although KO mice have greater cortical area (CA), the proportion of cortical area to the whole section, as described by percent cortical area (%CA) was not significantly different between the groups (Table 4, Figures 10, 11 (B)). Additionally, the shape of the cortical cross-section that describes the distribution of cortical bone (I_{max}/I_{min}) was not significantly different between the groups (Table 4, Figures 10, 11 (D)). These results indicate that KO femora and humeri are thicker than WT, but that the proportion and distribution of cortical bone are similar between groups.

Table 4. Standardized Cross-Sectional Properties, WT vs KO

All t-tests assumed unequal variances between groups. Therefore, a Welch's t-test was used. As sample sizes were small, a Wilcoxon rank sum test was also used. (Results coincide between tests). All data were normally distributed.

J, polar second moment of area; CA, cortical area; %CA, percent cortical area; I_{max}, maximum second moment of area; I_{min}, minimum second moment of area; I_{max}/I_{min}, diaphyseal shape.

| Cross-Sectional Property | Summary Statistics | | | | | | Welch's t-test | | Wilcoxon Rank Sum Test | |
	N	WT Mean	SD	N	KO Mean	SD	t score	p value	W	p value
Femur J	8	**0.13**	0.016	8	**0.19**	0.026	5.72	**0.00010 ***	**0**	**0.00016 ***
Femur CA	8	**56.91**	3.71	8	**70.53**	5.88	5.54	**0.00012 ***	**0**	**0.00016 ***
Femur %CA	8	66.76	1.8	8	69.17	4.33	1.45	0.18	19	0.19
Femur I_{max}/I_{min}	8	1.97	0.13	8	2.00	0.20	0.26	0.80	29	0.80
Humerus J	8	**0.049**	0.005	8	**0.060**	0.007	3.78	**0.002 ***	**7**	**0.007 ***
Humerus CA	8	**33.01**	2.68	8	**36.43**	2.57	2.60	**0.021**	**12**	**0.04**
Humerus %CA	8	83.15	1.49	8	83.16	2.15	0.014	0.99	26	0.57
Humerus I_{max}/I_{min}	8	1.41	0.1	8	1.36	0.09	0.97	0.35	42	0.33

Femur: Cross-Sectional Geometry
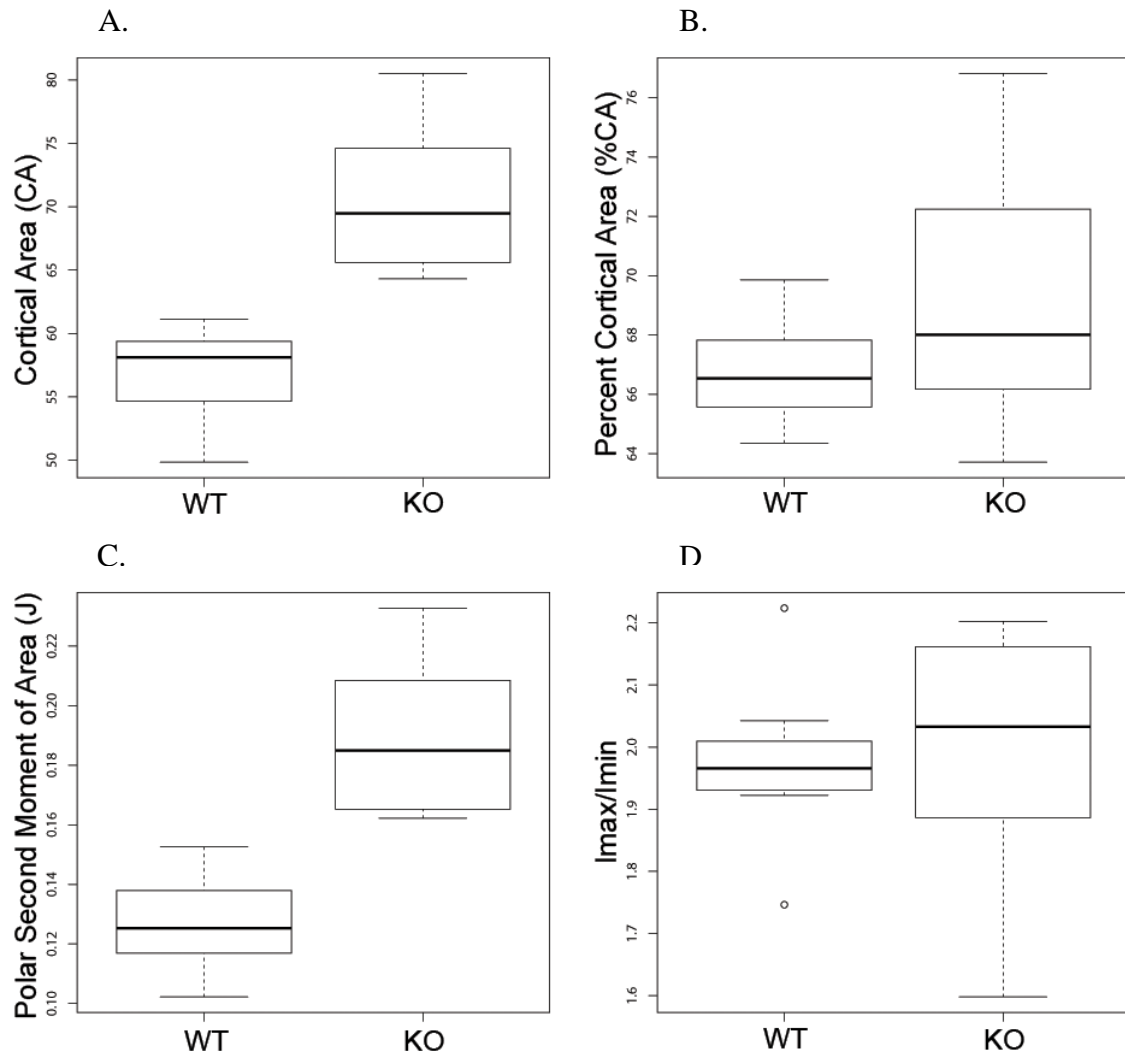
Figure 10. (A) Femur cortical area, (B) Femur percent cortical area (cortical area/total subperiosteal area X 100), (C) Femur midshaft torsional rigidity (J), and (D) Femur midshaft shape (I_{max}/I_{min}). All values have been standardized by body size. Boxes represent the 25th-75th percentile range, with the horizontal dark line indicating the median; whiskers extending to the maximum and minimum values within 1.5 box lengths. Outliers are indicated by °.

Humerus: Cross-Sectional Geometry
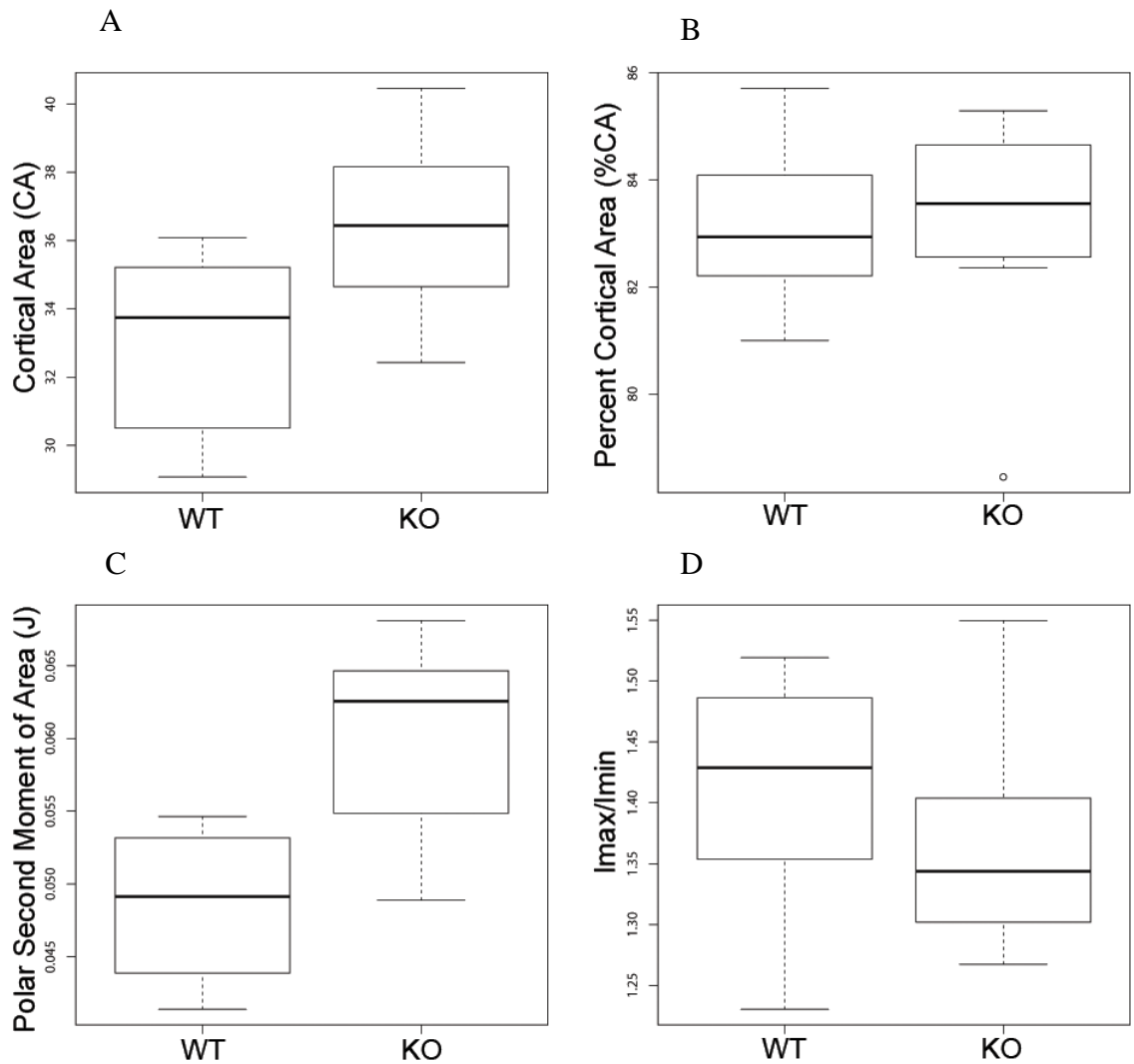
Figure 11. (A) Humerus cortical area, (B) Humerus percent cortical area (cortical area/total subperiosteal area X 100), (C) Humerus midshaft torsional rigidity (J), and (D) Humerus midshaft shape (I_{max}/I_{min}). All values have been standardized by body size. Boxes represent the 25th-75th percentile range, with the horizontal dark line indicating the median; whiskers extending to the maximum and minimum values within 1.5 box lengths. Outliers are indicated by ∘.

5   Discussion

The pannexin family of channel forming glycoproteins has received increasing attention as their diverse roles in physiology and disease continue to be uncovered. Of the three members of this family, Panx3 has been the least studied, in part, owing to its limited expression profile. Current research finds Panx3 is highly expressed in skeletal tissues; in growing long bones, it is induced at the growth plate where it has a role in regulation of proliferation and differentiation of cartilage and bone-forming cells.

This study analyzed the phenotypic aspects of humeri and femora in a novel knockout mouse that is devoid of Panx3 in all tissues. Results find distinct shape differences between the long bones of the Panx3 KO mouse compared to wildtype controls. PCA analysis indicates that a significant portion of this shape difference (20-30% for the femora and humeri respectively) is attributed to the allometric component of shape.

Analysis of landmark coordinate data using EDMA then brought to light the nature and magnitude of some of these proportional differences between KO and WT long bones. In the EDMA "form" analysis, which includes all size components of the landmark configurations, approximately half of the interlandmark distances were significantly different between the two groups for both humeral and femoral form analyses. Of these significantly different distances, all (but one) were larger in WT mice than in the KO mice. All of these distances that were larger in WT involved measures of diaphyseal length. From this analysis, it is concluded that the long bones of the WT mice have longer diaphyses than those of KO mice when scale is included. Length measures obtained from CT data confirmed a significant overall bone length difference between the two groups. In EDMA "shape" analysis, a scaling factor is used to "size-correct" configurations to elucidate differences that can be overwhelmed when scale is included. Once scaled in this manner, over half of the distances were significantly different between groups for both

long bones analyzed. Of those significantly different distances, a notable number (25% in femur and 47% in humerus) were larger in KO than in WT. The majority of distances that were larger in KO in the shape analysis span from the proximal metaphysis to a bony prominence for large muscle attachment (third trochanter in femur, deltoid tuberosity in humerus). With the exception of two distances in the humerus, the remainder of the distances that were significantly greater in KO than WT were within the third trochanter/deltoid tuberosity or within the ephiphyses. In shape analysis as with form analysis, all of the distances that were greater in WT than in KO mice were measures of diaphyseal length. From shape analysis it is concluded that WT mice have proportionally greater measures of diaphysis length than KO mice, and KO mice have proportionally larger regions of muscle attachment and epiphyses than WT mice.

The compromised length of long bones noted in KO mice may be explained on the basis of inhibited growth plate expansion in the absence of Panx3. Expression of Panx3 at the growth plate promotes the differentiation of chondrocytes to a mature form that begins the process of mineralization of the matrix, which is necessary for subsequent bone deposition. Panx3 also mediates osteoblast differentiation. Interruption of this process of cartilage growth and replacement by bone as may occur in the absence of Panx3 would explain compromised longitudinal growth of the bone.

The variance in distances did not differ significantly between groups for either long bone. These results suggest that while the loss of Panx3 exerts a phenotypic effect on long bones, the effect is consistent. These results are in stark contrast to studies of mutant phenotypes.

The consistent variability in distances within each group suggests that the mechanisms at play effect altered proportions of the long bones reliably and any compensatory mechanisms influencing growth are not haphazard.

Body weight and BMD between WT and KO mice were compared to rule out the possibility that long bones in WT mice were larger due simply to a more robust body size or that they were different in quality due to their density and mineralization. No statistically significant difference was evident for body weight or BMD between the groups at the time of scanning. Therefore, the differences in bone shape do not appear to be related to overall body mass. As well, although Panx3 appears to affect the bone shape, mineralization does not appear to be affected. Panx3 promotes the differentiation of chondrocytes and osteoblasts that is required for bone mineralization, however, even in the absence of Panx3, mechanisms must be in place that allow for the collection of factors such as alkaline phosphatase, that are necessary for adequate mineralization.

Results of cross-sectional geometric property analyses indicate differences in bone distribution between groups. The cross-sectional geometry of long bones can predict mechanical properties of bones such as strength and rigidity (Ruff and Hayes 1983). The second polar moment of area (J) and cortical bone area (CA) were significantly greater in KO mice than in WT mice. These results indicate that the long bones of KO mice have greater torsional (J) and compressive (CA) resistance than WT mice. Cross-sectional shape (I_{max}/I_{min}) and the percentage of cortical bone area to total cross-sectional area (%CA) were not significantly different between groups indicating a consistently thicker diaphyseal cross-section in the long bones of the KO mice. As body weight and bone mineral density did not differ significantly between groups, the more robust diaphysis of KO mice cannot be explained on those grounds. As well, both groups of mice were similarly housed and there were no overt differences in their patterns or levels of activity.

A previous experiment by Ishikawa et al (2011) found that ex vivo growth of a murine newborn metatarsus in the presence of a Panx3 channel inhibitor resulted in compromised growth in both length and width. While the results of our current study were congruent with compromised longitudinal growth, in contrast to this ex vivo preparation, we found that in vivo, Panx3 null individuals demonstrated thicker diaphyses. As well, it is of note

that gross measurement of long bones in Panx3 KO mice up to 6 weeks of age did not demonstrate any anomalies in previous studies by Moon et. al (2015). Taken together, these results may suggest that in the absence of Panx3, long bone size is not compromised during development, but optimal growth may require Panx3. Alternatively, the difference in murine long bone size in vivo may be too subtle to detect by gross measurement and require increased measurement precision as provided by micro-CT imaging.

Results of our study suggest that Panx3 affects bone differently depending on the location and/or type of bone involved. We found decreased bone length, suggesting compromised longitudinal growth which implicates inhibition of the process of endochondral ossification at the growth plate. However, KO mice were proportionally larger than WT mice in areas that are mainly comprised of trabecular bone such as metaphyses/epiphyses and large muscle attachment sites. Additionally, KO mice had greater cross-sectional cortical area of diaphyses than WT mice.

In long bones, deposition of bone can occur on various surfaces. In periosteal ossification, osteogenic cells deposit bone on the periosteum (outer layer); in endosteal ossification bone is deposited by cells on the endosteum (inner bone layer); in perichondral ossification bone is deposited on mineralized cartilage by osteogenic cells brought into the marrow cavity; and in endochondral ossification, mineralized cartilage is resorbed and bone is deposited on cartilaginous spicules (Hall, 2005). Deposition of cortical bone in the diaphysis is accomplished by periosteal ossification where growth is appositional (deposited on top of an existing surface). However, in the metaphysis, it appears that cortical bone is created from the endosteal surface when trabeculae (formed by endochondral ossification) in the periphery of the growth plate enlarge and "coalesce" (Cadet et al. 2003). This process appears to increase both cortical girth and length in the metaphysis. Bone resorption then occurs at the periosteal surface to reduce the metaphyseal surface to the width of the diaphysis. Trabeculae formed nearer to the centre

of the growth plate are greatly resorbed to form the marrow cavity. There is increased osteoblast density at the peripheral trabeculae that appear to be responsible for the enlargement and coalescence of trabeculae at the periphery; the increased osteoblast density may be induced by, as yet unknown factors, from the periosteum (Cadet et al. 2003).

Trabecular bone is present in the epiphyses and metaphyses, as well as muscle attachment sites (ie. trochanters and tuberosities) of long bones. Cortical bone forms the outer shell of long bones and largely makes up the diaphysis. Proportional differences seen in this study may be related to the processes that regulate the differential deposition and/or resorption of trabecular and cortical bone in different regions of the bone.

Panx3 is known to regulate proliferation of osteoprogenitor cells and chondrocytes and to regulate differentiation of osteoblasts and chondrocytes. Perhaps its effect on these cells depends on the ossification process: ie. cortical vs trabecular, endosteal vs periosteal. It is also not yet known if Panx3 affects osteoclasts and hence if Panx3 has an effect on bone resorption and remodeling through regulation of these cells.

Another consideration is that the proportionally larger muscle attachment prominences of KO mice may be the result of increased strain on these areas due to differential muscle loading. Two species of Panx3 have been identified in skeletal muscle; the species are differentially expressed in undifferentiated skeletal muscle cells and myoblasts where they have a role in regulation of myoblast proliferation and differentiation (Langlois et al. 2014). As the Panx3 KO mouse line used in this study lacks the protein in all tissues, these mice may demonstrate differences in muscle properties related to its ablation that result in changes in the direction, intensity or frequency of muscle action. A difference in muscle mass, muscle attachments or density of muscle fibres may contribute to the long bone phenotype observed in this study. Alternatively, the bone in the KO mice may be

more sensitive to mechanical strain, causing an "over-reaction" of bone deposition in response to otherwise typical muscle loading.

5.1 Future Directions

Long bone shape is greatly influenced through muscle-bone interactions. The proportionately larger deltoid tuberosities and third trochanters in the KO mice in this study suggest that differences in muscle-bone interactions between the two groups could be responsible for the phenotypic differences observed. Thus, a comparison of muscle phenotypes between KO and WT mice may add to our understanding of the role of Panx3 in long bone growth and development. KO mice may have overall increased lean mass, increased bulk in a subset of muscles, or differences in muscle quality. Due to the effects of muscle-bone interactions, changes in muscle quantity and/or quality could be responsible for the bony changes observed in this study.

Determining if the expression of Panx3 differs by bone surface and/or type (cortical vs trabecular) may help determine whether its role varies depending on the region of the bone or type of bone. As well, determining whether or not Panx3 is expressed by osteoclasts or whether or not it is also associated with pathways involved in processes of resorption will help determine whether Panx3 influences long bone phenotype through regulating resorption as well as deposition.

Pannexin biology is a yet young and evolving area of research that holds promise for furthering understanding in processes of development, growth, and degeneration with implications for unraveling complexities associated with disease and evolutionary change. Aspects of long bones that are more prone to altered phenotype may be more vulnerable to change under genetic or environmental stress. Therefore, factors such as

Panx3 that influence skeletal phenotype may prove useful in applications for prevention and treatment of developmental or degenerative bone and joint dysfunction. Elucidation of Panx3's role in bone biology may also further research into buffering mechanisms that ensure a functional phenotype in spite of genetic anomaly, and determine aspects of phenotype most given to disruption and therefore most prone to evolutionary change. In the study of physiology, developmental and degenerative disease and in probing the mechanisms of evolutionary change, the pannexins are implicated as prime targets of focus in future research endeavours.

References

Akiyama H, Chaboissier M-C, Martin JF, Schedl A, Crombrugghe B de. 2002. The transcription factor Sox9 has essential roles in successive steps of the chondrocyte differentiation pathway and is required for expression of Sox5 and Sox6. Genes Dev 16:2813–2828.

Alberts B ed. 2008. Molecular biology of the cell. 5th ed. New York: Garland Science.

Ambrosi C, Gassmann O, Pranskevich JN, Boassa D, Smock A, Wang J, Dahl G, Steinem C, Sosinsky GE. 2010. Pannexin1 and Pannexin2 Channels Show Quaternary Similarities to Connexons and Different Oligomerization Numbers from Each Other. J Biol Chem 285:24420–24431.

Amizuka N, Hasegawa T, Oda K, Luiz de Freitas PH, Hoshi K, Li M, Ozawa H. 2012. Histology of epiphyseal cartilage calcification and endochondral ossification. Front Biosci Elite Ed 4:2085–2100.

Anderson HC. 1969. Vesicles Associated With Calcification In the Matrix of Epiphyseal Cartilage. J Cell Biol 41:59.

Baab KL, McNulty KP, Rohlf FJ. 2012. The shape of human evolution: A geometric morphometrics perspective. Evol Anthropol Issues News Rev 21:151–165.

Bao L, Locovei S, Dahl G. 2004. Pannexin membrane channels are mechanosensitive conduits for ATP. FEBS Lett 572:65–68.

Baranova A, Ivanov D, Petrash N, Pestova A, Skoblov M, Kelmanson I, Shagin D, Nazarenko S, Geraymovych E, Litvin O, Tiunova A, Born TL, Usman N, Staroverov D, Lukyanov S, Panchin Y. 2004. The mammalian pannexin family is homologous to the invertebrate innexin gap junction proteins. Genomics 83:706–716.

Beaucage KL, Xiao A, Pollmann SI, Grol MW, Beach RJ, Holdsworth DW, Sims SM, Darling MR, Dixon SJ. 2014. Loss of P2X7 nucleotide receptor function leads to abnormal fat distribution in mice. Purinergic Signal 10:291–304.

Behrens J, von Kries JP, Kühl M, Bruhn L, Wedlich D, Grosschedl R, Birchmeier W. 1996. Functional interaction of β-catenin with the transcription factor LEF-1. Nature 382:638–642.

Bertram JEA, Swartz SM. 1991. The "law of Bone Transformation": A Case of Crying Wolff? Biol Rev 66:245–273.

Bi W, Deng JM, Zhang Z, Behringer RR, de Crombrugghe B. 1999. Sox9 is required for cartilage formation. Nat Genet 22:85–89.

Boassa D, Ambrosi C, Qiu F, Dahl G, Gaietta G, Sosinsky G. 2007. Pannexin1 Channels Contain a Glycosylation Site That Targets the Hexamer to the Plasma Membrane. J Biol Chem 282:31733–31743.

Bond SR, Lau A, Penuela S, Sampaio AV, Underhill TM, Laird DW, Naus CC. 2011. Pannexin 3 is a novel target for Runx2, expressed by osteoblasts and mature growth plate chondrocytes. J Bone Miner Res 26:2911–2922.

Bond SR, Naus CC. 2014. The pannexins: past and present. Front Physiol 5:58.

Bruzzone R, Barbe MT, Jakob NJ, Monyer H. 2005. Pharmacological properties of homomeric and heteromeric pannexin hemichannels expressed in Xenopus oocytes. J Neurochem 92:1033–1043.

Bruzzone R, Hormuzdi SG, Barbe MT, Herb A, Monyer H. 2003. Pannexins, a family of gap junction proteins expressed in brain. Proc Natl Acad Sci 100:13644–13649.

Burr DB, Robling AG, Turner CH. 2002. Effects of biomechanical stress on bones in animals. Bone 30:781–786.

Burstein AH, Wright TM. 1994. Fundamentals of orthopaedic biomechanics. Baltimore: Williams & Wilkins.

Cadet ER, Gafni RI, McCarthy EF, McCray DR, Bacher JD, Barnes KM, Baron J. 2003. Mechanisms Responsible for Longitudinal Growth of the Cortex: Coalescence of Trabecular Bone into Cortical Bone. J Bone Jt Surg 85:1739–1748.

Carlson KJ, Judex S. 2007. Increased non-linear locomotion alters diaphyseal bone shape. J Exp Biol 210:3117–3125.

Celetti SJ, Cowan KN, Penuela S, Shao Q, Churko J, Laird DW. 2010. Implications of pannexin 1 and pannexin 3 for keratinocyte differentiation. J Cell Sci 123:1363–1372.

Cole III T. 2002. MIBoot Windows-based software for booststrapbased comparison of morphologial integration patterns. Richtsmeier Lab. Available at: http://getahead.psu.edu.

Cowan KN, Langlois S, Penuela S, Cowan BJ, Laird DW. 2012. Pannexin1 and Pannexin3 Exhibit Distinct Localization Patterns in Human Skin Appendages and are Regulated during Keratinocyte Differentiation and Carcinogenesis. Cell Commun Adhes 19:45–53.

De Crombrugghe B, Lefebvre V, Behringer RR, Bi W, Murakami S, Huang W. 2000. Transcriptional mechanisms of chondrocyte differentiation. Matrix Biol 19:389–394.

Daegling DJ. 2002. Estimation of torsional rigidity in primate long bones. J Hum Evol 43:229–239.

Fang X, Yu SX, Lu Y, Bast RC, Woodgett JR, Mills GB. 2000. Phosphorylation and inactivation of glycogen synthase kinase 3 by protein kinase A. Proc Natl Acad Sci 97:11960–11965.

Fedde KN, Blair L, Silverstein J, Coburn SP, Ryan LM, Weinstein RS, Waymire K, Narisawa S, Millán JL, Macgregor GR, Whyte MP. 1999. Alkaline Phosphatase Knock-Out Mice Recapitulate the Metabolic and Skeletal Defects of Infantile Hypophosphatasia. J Bone Miner Res 14:2015–2026.

Frelat MA, Katina S, Weber GW, Bookstein FL. 2012. Technical note: A novel geometric morphometric approach to the study of long bone shape variation. Am J Phys Anthropol 149:628–638.

Glass DA, Bialek P, Ahn JD, Starbuck M, Patel MS, Clevers H, Taketo MM, Long F, McMahon AP, Lang RA, Karsenty G. 2005. Canonical Wnt signaling in differentiated osteoblasts controls osteoclast differentiation. Dev Cell 8:751–764.

Granton PV, Norley CJD, Umoh J, Turley EA, Frier BC, Noble EG, Holdsworth DW. 2010. Rapid in vivo whole body composition of rats using cone beam μCT. J Appl Physiol 109:1162–1169.

Hall BK. 2005. *Chapter 2 Bone* In: *Bones and cartilage: developmental and evolutionary skeletal biology*. San Diego, Calif. ; London: Elsevier Academic Press pp 21-22.

Huiskes R. 1982. On the modelling of long bones in structural analyses. J Biomech 15:65–69.

Ishikawa M, Iwamoto T, Fukumoto S, Yamada Y. 2014. Pannexin 3 Inhibits Proliferation of Osteoprogenitor Cells by Regulating Wnt and p21 Signaling. J Biol Chem 289:2839–2851.

Ishikawa M, Iwamoto T, Nakamura T, Doyle A, Fukumoto S, Yamada Y. 2011. Pannexin 3 functions as an ER Ca2+ channel, hemichannel, and gap junction to promote osteoblast differentiation. J Cell Biol 193:1257–1274.

Iwamoto T, Nakamura T, Doyle A, Ishikawa M, Vega S de, Fukumoto S, Yamada Y. 2010. Pannexin 3 Regulates Intracellular ATP/cAMP Levels and Promotes Chondrocyte Differentiation. J Biol Chem 285:18948–18958.

Kato M, Patel MS, Levasseur R, Lobov I, Chang BH-J, Glass DA, Hartmann C, Li L, Hwang T-H, Brayton CF, Lang RA, Karsenty G, Chan L. 2002. Cbfa1-independent decrease in osteoblast proliferation, osteopenia, and persistent embryonic eye vascularization in mice deficient in Lrp5, a Wnt coreceptor. J Cell Biol 157:303–314.

Katzenberg MA, Saunders SR eds. 2008. *Chapter 6 Biomechanical analyses of archaeological human skeletons. In: Biological anthropology of the human skeleton*. 2nd ed. Hoboken, N.J: Wiley-Liss, pp 183-190.

Komori T, Yagi H, Nomura S, Yamaguchi A, Sasaki K, Deguchi K, Shimizu Y, Bronson RT, Gao Y-H, Inada M, Sato M, Okamoto R, Kitamura Y, Yoshiki S, Kishimoto T. 1997. Targeted Disruption of Cbfa1 Results in a Complete Lack of Bone Formation owing to Maturational Arrest of Osteoblasts. Cell 89:755–764.

Kronenberg HM. 2003. Developmental regulation of the growth plate. Nature 423:332–336.

Lai CPK, Bechberger JF, Naus CC. 2009. Pannexin2 as a novel growth regulator in C6 glioma cells. Oncogene 28:4402–4408.

Langlois S, Xiang X, Young K, Cowan BJ, Penuela S, Cowan KN. 2014. Pannexin 1 and Pannexin 3 Channels Regulate Skeletal Muscle Myoblast Proliferation and Differentiation. J Biol Chem 289:30717–30731.

Lele S. 1995. Euclidean distance matrix analysis: Confidence intervals for form and growth differences. Am J Phys Anthropol 98:73–86.

Lele S, Richtsmeier JT. 2001. An invariant approach to statistical analysis of shapes: interdisciplinary statistics. Boca Raton, Fla. ; London: Chapman & Hall/CRC.

Lieberman DE, Devlin MJ, Pearson OM. 2001. Articular area responses to mechanical loading: effects of exercise, age, and skeletal location. Am J Phys Anthropol 116:266–277.

Lieberman DE, Polk JD, Demes B. 2004. Predicting long bone loading from cross-sectional geometry. Am J Phys Anthropol 123:156–171.

Long F, Ornitz DM. 2013. Development of the Endochondral Skeleton. Cold Spring Harb Perspect Biol 5:a008334.

Macdonald HM, Cooper DML, McKay HA. 2008. Anterior–posterior bending strength at the tibial shaft increases with physical activity in boys: evidence for non-uniform geometric adaptation. Osteoporos Int 20:61–70.

Mackie EJ, Ahmed YA, Tatarczuch L, Chen K-S, Mirams M. 2008. Endochondral ossification: How cartilage is converted into bone in the developing skeleton. Int J Biochem Cell Biol 40:46–62.

Minina E, Kreschel C, Naski MC, Ornitz DM, Vortkamp A. 2002. Interaction of FGF, Ihh/Pthlh, and BMP Signaling Integrates Chondrocyte Proliferation and Hypertrophic Differentiation. Dev Cell 3:439–449.

Moon P, Penuela S, Barr K, Pin C, Welch I, Attur M, Abramson S, Beier F. 2015. Cartilage-specific deletion of Panx3 prevents the development of surgically induced osteoarthritis. J Mol Med In Revision.

Naski MC, Colvin JS, Coffin JD, Ornitz DM. 1998. Repression of hedgehog signaling and BMP4 expression in growth plate cartilage by fibroblast growth factor receptor 3. Development 125:4977–4988.

Nunamaker DM, Butterweck DM, Provost MT. 1990. Fatigue fractures in thoroughbred racehorses: Relationships with age, peak bone strain, and training. J Orthop Res 8:604–611.

Ornitz DM, Marie PJ. 2002. FGF signaling pathways in endochondral and intramembranous bone development and human genetic disease. Genes Dev 16:1446–1465.

Otto F, Thornell AP, Crompton T, Denzel A, Gilmour KC, Rosewell IR, Stamp GWH, Beddington RSP, Mundlos S, Olsen BR, Selby PB, Owen MJ. 1997. Cbfa1, a Candidate Gene for Cleidocranial Dysplasia Syndrome, Is Essential for Osteoblast Differentiation and Bone Development. Cell 89:765–771.

Panchin Y, Kelmanson I, Matz M, Lukyanov K, Usman N, Lukyanov S. 2000. A ubiquitous family of putative gap junction molecules. Curr Biol 10:R473–R474.

Pearson OM, Lieberman DE. 2004. The aging of Wolff's "law": Ontogeny and responses to mechanical loading in cortical bone. Am J Phys Anthropol 125:63–99.

Penuela S, Bhalla R, Gong X-Q, Cowan KN, Celetti SJ, Cowan BJ, Bai D, Shao Q, Laird DW. 2007. Pannexin 1 and pannexin 3 are glycoproteins that exhibit many distinct characteristics from the connexin family of gap junction proteins. J Cell Sci 120:3772–3783.

Penuela S, Bhalla R, Nag K, Laird DW. 2009. Glycosylation Regulates Pannexin Intermixing and Cellular Localization. Mol Biol Cell 20:4313–4323.

Penuela S, Gehi R, Laird DW. 2013. The biochemistry and function of pannexin channels. Biochim Biophys Acta BBA - Biomembr 1828:15–22.

Penuela S, Harland L, Simek J, Laird DW. 2014. Pannexin channels and their links to human disease. Biochem J 461:371–381.

Reilly DT, Burstein AH. 1974. The Mechanical Properties of Cortical Bone. J Bone Jt Surg 56:1001–1022.

Richtsmeier JT, Cole TM, Krovitz G, Valeri CJ, Lele S. 1998. Preoperative morphology and development in sagittal synostosis. J Craniofac Genet Dev Biol 18:64–78.

Robling AG, Hinant FM, Burr DB, Turner CH. 2002. Improved Bone Structure and Strength After Long-Term Mechanical Loading Is Greatest if Loading Is Separated Into Short Bouts. J Bone Miner Res 17:1545–1554.

Rohlf FJ, Slice D. 1990. Extensions of the Procrustes Method for the Optimal Superimposition of Landmarks. Syst Biol 39:40–59.

Ross MH, Pawlina W. 2011. Histology: a text and atlas: with correlated cell and molecular biology. 6th ed. Philadelphia: Wolters Kluwer/Lippincott Williams & Wilkins Health.

Ruff CB. 2002. Long bone articular and diaphyseal structure in old world monkeys and apes. I: Locomotor effects. Am J Phys Anthropol 119:305–342.

Ruff CB, Hayes WC. 1983. Cross-sectional geometry of Pecos Pueblo femora and tibiae--a biomechanical investigation: I. Method and general patterns of variation. Am J Phys Anthropol 60:359–381.

Ruff C, Holt B, Trinkaus E. 2006. Who's afraid of the big bad Wolff?: "Wolff's law" and bone functional adaptation. Am J Phys Anthropol 129:484–498.

Scemes E, Spray DC, Meda P. 2008. Connexins, pannexins, innexins: novel roles of "hemi-channels." Pflüg Arch - Eur J Physiol 457:1207–1226.

Seo JH, Jin Y-H, Jeong HM, Kim Y-J, Jeong HG, Yeo C-Y, Lee K-Y. 2009. Calmodulin-dependent kinase II regulates Dlx5 during osteoblast differentiation. Biochem Biophys Res Commun 384:100–104.

Shaw CN, Stock JT. 2009a. Habitual throwing and swimming correspond with upper limb diaphyseal strength and shape in modern human athletes. Am J Phys Anthropol 140:160–172.

Shaw CN, Stock JT. 2009b. Intensity, repetitiveness, and directionality of habitual adolescent mobility patterns influence the tibial diaphysis morphology of athletes. Am J Phys Anthropol 140:149–159.

Smits P, Dy P, Mitra S, Lefebvre V. 2004. Sox5 and Sox6 are needed to develop and maintain source, columnar, and hypertrophic chondrocytes in the cartilage growth plate. J Cell Biol 164:747–758.

Smits P, Li P, Mandel J, Zhang Z, Deng JM, Behringer RR, de Crombrugghe B, Lefebvre V. 2001. The Transcription Factors L-Sox5 and Sox6 Are Essential for Cartilage Formation. Dev Cell 1:277–290.

Sosinsky GE, Boassa D, Dermietzel R, Duffy HS, Laird DW, MacVicar B, Naus CC, Penuela S, Scemes E, Spray DC, Thompson RJ, Zhao H-B, Dahl G. 2011. Pannexin channels are not gap junction hemichannels. Channels 5:193–197.

St-Jacques B, Hammerschmidt M, McMahon AP. 1999. Indian hedgehog signaling regulates proliferation and differentiation of chondrocytes and is essential for bone formation. Genes Dev 13:2072–2086.

Stock JT, Shaw CN. 2007. Which measures of diaphyseal robusticity are robust? A comparison of external methods of quantifying the strength of long bone diaphyses to cross-sectional geometric properties. Am J Phys Anthropol 134:412–423.

Sumner-Smith G (Geoff), Bishop HM (Helen M) eds. 1982. Bone in clinical orthopaedics: a study in comparative osteology. Philadelphia: Saunders.

Suzuki A, Ozono K, Kubota T, Kondou H, Tachikawa K, Michigami T. 2008. PTH/cAMP/PKA signaling facilitates canonical Wnt signaling via inactivation of glycogen synthase kinase-3β in osteoblastic Saos-2 cells. J Cell Biochem 104:304–317.

Trinkaus E, Churchill SE, Villemeur I, Riley KG, Heller JA, Ruff CB. 1991. Robusticity versus Shape: The Functional Interpretation of Neandertal Appendicular Morphology. J Anthropol Soc Nippon 99:257–278.

Turmel P, Dufresne J, Hermo L, Smith CE, Penuela S, Laird DW, Cyr DG. 2011. Characterization of pannexin1 and pannexin3 and their regulation by androgens in the male reproductive tract of the adult rat. Mol Reprod Dev 78:124–138.

White A, Wallis G. 2001. Endochondral ossification: A delicate balance between growth and mineralisation. Curr Biol 11:R589–R591.

Woo SL, Kuei SC, Amiel D, Gomez MA, Hayes WC, White FC, Akeson WH. 1981. The effect of prolonged physical training on the properties of long bone: a study of Wolff's Law. J Bone Jt Surg 63:780–787.

Yen MR, Saier Jr MH. 2007. Gap junctional proteins of animals: The innexin/pannexin superfamily. Prog Biophys Mol Biol 94:5–14.

Yoon BS, Pogue R, Ovchinnikov DA, Yoshii I, Mishina Y, Behringer RR, Lyons KM. 2006. BMPs regulate multiple aspects of growth-plate chondrogenesis through opposing actions on FGF pathways. Development 133:4667–4678.

Yoshida CA, Yamamoto H, Fujita T, Furuichi T, Ito K, Inoue K, Yamana K, Zanma A, Takada K, Ito Y, Komori T. 2004. Runx2 and Runx3 are essential for chondrocyte maturation, and Runx2 regulates limb growth through induction of Indian hedgehog. Genes Dev 18:952–963.

Zayzafoon M, Fulzele K, McDonald JM. 2005. Calmodulin and Calmodulin-dependent Kinase IIα Regulate Osteoblast Differentiation by Controlling c-fos Expression. J Biol Chem 280:7049–7059.

Zelditch ML, Swiderski DL, Sheets HD. 2012. Geometric Morphometrics for Biologists: A Primer. Academic Press.

Morphometric analyses were performed in Morpho-J, version 1.06c (C. P. Klingenberg. 2011). MorphoJ: an integrated software package for geometric morphometrics. Molecular Ecology Resources 11: 353-357.

doi: 10.1111/j.1755-0998.2010.02924.x).

Supplementary Tables

Table 5. Femur Form Data
       Distances that are Significantly Larger in WT than KO

Landmark	Landmark	Percentage Difference
in	gtp	2-6 ◊
in	pitf	1 ◊
in	ptt	2-6
gtp	mep	2-7 ◊
pitf	mep	1-8
in	tgta	2-7
ptt	mep	2-8 ◊
in	gtl	3-7
in	gts	3-7
ptt	mps	3-8
pitf	mps	2-9
tgta	mep	3-8
gtp	mps	3-8
ptt	lep	3-8
ptt	lps	3-8
tgta	lep	4-8
tgta	mps	3-8
gtl	mep	3-8
gts	lep	4-8
gts	mep	3-8
gts	mps	4-8
gtl	lep	4-8
pitf	lep	3-9
gtl	mps	4-8
pitf	lps	3-9 ◊
tgta	lps	4-8
in	ditc	4-8
gts	lps	4-8
in	dtt	3-9
dtt	mep	3-10
gtl	lps	4-8
in	ltsd	4-9
gtp	lep	4-9
gtp	lps	4-9
ditc	mps	5-10*
ditc	mep	4-10
ltsd	mep	4-10
ltsd	mps	5-10*
ditc	lep	5-10*
ditc	lps	5-10*
dtt	mps	4-11

ltsd	lps	6-10*
ltsd	lep	6-11*
dtt	lps	6-13*
dtt	lep	7-13*

Table 6. Femur Form Data
Distances that are Significantly Larger in KO than WT

Landmark	Landmark	Percentage Difference
in	lep	1-8*

* Distances that are diagrammed in Figure 5.

◊ Distances that are significantly correlated with age.

Table 7. Humerus Form Data
Distances that are Significantly
Larger in WT than in KO

Landmark	Landmark	Percentage Difference
sc	mep	1- 6
ins	lep	2- 6
pgp	lep	3-6
lgtgp	hlt	1 - 9
mltgp	lep	3 - 7
tdt	lep	3 - 8 ◊
pdt	lep	3- 8 ◊
lgtgp	lep	4 - 7
hlt	lep	4 - 8
ins	sc	5 – 9*
pgp	sc	5.5 - 9.6*
mltgp	sc	6 – 10*
ins	cf	7 – 11*
lgtgp	sc	7 – 11*
pdt	sc	6 – 12 ◊
ddt	lep	7 – 11*
pgp	cf	7 – 12*
hlt	sc	7 – 12*
mltgp	cf	8 – 13*
lgtgp	cf	8 – 13*
hlt	cf	8 – 13*
tdt	sc	7 – 15*
pdt	cf	9 – 14 ◊
ins	mep	10 – 14*
pgp	mep	10 – 14*
hlt	mep	10 – 15*
lgtgp	mep	11 – 15*
mltgp	mep	11 – 16*
tdt	cf	11 – 19*
pdt	mep	12 – 18*
ddt	sc	14 – 20*
tdt	mep	15 – 23*
ddt	cf	16 – 23*
ddt	mep	19 – 26*

* Distances that are diagrammed in Figure 6.

◊ Distances that are significantly correlated

with age

Table 8. Femur Shape Data
Distances that are Significantly
Larger in WT than in KO

Landmark	Landmark	Percentage Difference
gtp	mps	1 - 7
ptt	mps	1-6
in	tgta	1-6
in	gtl	2-7
dtt	mep	1-9
in	gts	2-7
in	dtt	2-8
ptt	lps	2-7
ptt	lep	2-8
pitf	lep	1-9 ◊
pitf	lps	1-9
gtp	lep	2-8
gtp	lps	2-8
tgta	mep	2-9
tgta	mps	3-9
dtt	mps	3-9
tgta	lep	4-8
gtl	mep	2-10
gtl	mps	4-9
gtl	lep	4-9
in	ltsd	4-9
gts	lep	4-9
gts	mep	3-10
gts	mps	4-9
tgta	lps	4-9
in	ditc	4-9
gtl	lps	5-9
ltsd	mps	4-10
gts	lps	5-10*
ltsd	mep	4-11
dtt	lps	5-11*
ditc	mps	5-11*
ditc	mep	5-12*
dtt	lep	6-12*
ltsd	lps	6-11*
ditc	lep	6-12*
ditc	lps	6-12*
ltsd	lep	6-12*

* Distances that are diagrammed in Figure 6.

◊ Distances that are significantly correlated with age.

Table 9. Femur Shape Data
Distances that are Significantly Larger in KO than WT

Landmark	Landmark	Percentage Difference
gts	dtt	2-6*
ptt	dtt	2-7*
gtl	dtt	2-6 ◊
dtt	tgta	2-5*
pitf	dtt	1-6 ◊
gtp	dtt	0.5 – 5*
gts	gtp	0.5 – 5*
in	lep	0.4 - 4
gts	ltsd	1- 4
gts	ditc	1 - 4
gtp	ptt	0.1 – 5*
ditc	dtt	0.2 – 4 ◊
in	mep	0.1 - 3

* Distances that are diagrammed in Figure 6.

◊ Distances that are significantly correlated with age.

Table 10. Humerus Shape Data.
Distances that are Significantly Larger in WT than KO

Landmark	Landmark	Percentage Difference
ins	sc	1 - 5
pgp	sc	2 - 6
ddt	lep	3 - 6
mltgp	sc	3 - 7
tdt	sc	3 - 8
pdt	sc	4 – 9 ◊
lgtgp	sc	5 – 9*
hlt	sc	5 – 10*
ins	cf	6 – 8*
pgp	cf	7 – 9*
mltgp	cf	8 – 11*
ddt	sc	7 – 11*
lgtgp	cf	9 – 11*
tdt	cf	9 – 12*
hlt	cf	9 – 12*
pdt	cf	9- 13 ◊
ddt	cf	12 – 15*
ins	mep	12- 15*
pgp	mep	13 – 17*
hlt	mep	13 – 17*
lgtgp	mep	14 – 18*
mltgp	mep	14 – 18*
tdt	mep	15 – 18*
ddt	mep	17 – 20*
pdt	mep	16 – 21*

* Distances that are diagrammed in Figure 6.

◊ Distances that are significantly correlated with age.

Table 11. Humerus Shape Data
Distances that are Significantly Larger in KO than WT

Landmark	Landmark	Percentage Difference
ins	ddt	7.5 – 9*
ins	tdt	5.5 – 8*
mltgp	ddt	5 - 7.5*
pgp	ddt	5.2 – 7 ◊
hlt	ddt	3.3 – 7*
pgp	tdt	3.5 – 6*
mltgp	tdt	3 – 6*
lep	sc	3 - 5.6*
hlt	tdt	2 – 6*
pdt	ddt	2 – 5 ◊
lgtgp	ddt	2 – 5*
ins	pdt	2 – 5*
pgp	pdt	1 - 4.5
ins	lep	1 - 4.5
ins	hlt	1 - 4
lgtgp	tdt	1 - 4
lep	cf	1 - 4
ins	lgtgp	1 - 4
pdt	tdt	1 – 4 ◊
pgp	lep	0.5 - 4
lep	mep	.3 - 4
pgp	lgtgp	.5 - 4

* Distances that are diagrammed in Figure 6.

◊ Distances that are significantly correlated with age.

Table 12. Weight of Mice at Time of Scanning

KO Individual	Weight at Time of Scanning (g)	WT Individual	Weight at Time of Scanning (g)
KO1	21.5	WT1	24.3
KO2	23.1	WT2	24.7
KO3	25	WT3	24.6
KO4	25.4	WT4	23
KO5	25.5	WT5	28.5
KO6	27.1	WT6	25.6
KO7	24.8	WT7	24.6
KO8	25.9	WT8	31.2
KO9	24.3	WT9	31.3
KO10	23.6	WT10	25

Table 13. Length of Femora and Humeri at Time of Scanning

KO Individual	Length at Time of Scanning (mm)		WT Individual	Length at Time of Scanning (mm)	
	Femur	Humerus		Femur	Humerus
KO1	14.02	10.89	WT1	14.83	11.36
KO2	13.93	11.07	WT2	14.53	11.49
KO3	14.26	10.83	WT3	14.93	11.26
KO4	14.44	11.4	WT4	15.02	11.36
KO5	14.74	10.96	WT5	15.44	11.76
KO6	14.96	11.05	WT6	15.32	11.2
KO7	14.11	11.52	WT7	15.42	11.56
KO8	14.46	11.15	WT8	16	12.19
KO9	14.58	11.49	WT9	16.03	12.03
KO10	14.1	11.39	WT10	15.14	11.34

Appendices

Appendix A: Principal Components Analysis (PCA) Supplement

Reference (Zelditch, Swiderski, and Sheets 2012)

PCA is a data reduction method of data analysis that is helpful for simplifying the description of variation. The original variables are replaced with new variables (principal components) that describe the direction of greatest variance. Because the majority of the variation in a sample can usually be described with only a few principal components, the new variables simplify variation and also depict how the variation is distributed in the forms. PCA can be useful for visualization and interpretation of differences.

Principal components are the directions of greatest variance. Graphically, they are the directions where the data is most spread out.

Figure I shows data points for two observed traits, X and Y. Each point is the observation for a single specimen. First, the direction that describes the largest amount of the variance is found by finding the direction through the scatter where the data has the greatest spread. In Figure II, the ellipse enclosing the data points depicts the range of the variance. The long axis of the ellipse is the line where the data has the greatest spread. To minimize the variance that is not described, the line is drawn so as to minimize the sum of squared distances from the data points to the line (Figure III). This line is the first principal component that describes the maximum amount of variance among the points.
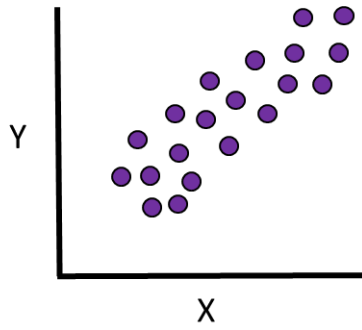
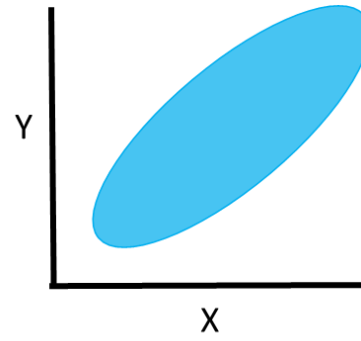Figure I : Scatter plot of individuals with two observed traits X and Y

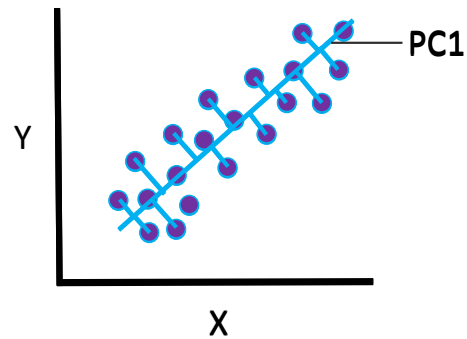Figure II: an ellipse enclosing the data points illustrates the range of variance of

Figure III: The line that can be drawn along the long axis of the ellipse that minimizes the squared distances of the data points to that line is the first principal component (PC1) representing the maximum portion of variance.

Figures modified from (Zelditch, Swiderski, and Sheets 2012)

In a simple case such as this example, because there are only two variables, all of the variation that is not described by the first axis (PC1) is described by the second axis of the ellipse (PC2). After the variation in the original variables has been described in terms of PCs, the next step is to determine the positions of the individuals relative to these new axes (Figure IV). The point where the PCs intersect is the sample mean. The PC scores represent the distances of the individual from the mean in the directions of the PCs. The PCs become the axes of a new coordinate system that allows us to view the data from a different perspective. The relative positions of the data points remain the same. These axes represent the direction where there is the most variation, and therefore the most information.
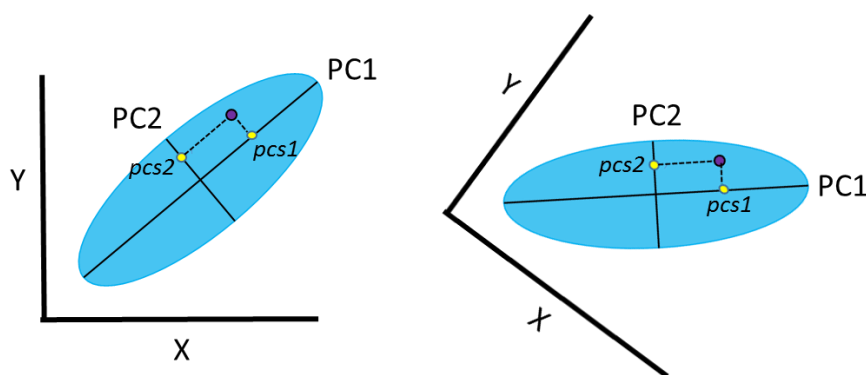
Figuew IV: The purple circle represents an individual data point in the sample. Pcs1 and pcs2 are the principal component scores of the individual on PC1 and PC2 that are distances from the mean (intersection of PC1 and PC2). Figures modified from (Zelditch, Swiderski, and Sheets 2012)

Math using eigenvectors and eigenvalues can be used to find the principal component rather than graphic representation. An eigenvector is a direction, for example, the slope of the line. Every eigenvector has an eigenvalue which is a number representing the extent of variance in that direction. The eigenvector with the highest eigenvalue is therefore the principal component. The number of eigenvectors/values that exist equal the number of

variables or dimensions of the data. In a 2-variable data set, PC1 is the first eigenvector and PC2 is the second.

PCA can be used to reduce the dimensions of the data to provide a view of the greatest variation while stripping away the unnecessary components. In a 3-variable data set for example, the first and second eigenvector would describe the vast majority of the variation and the third eigenvector would be very small so that it could be discarded from the view, thereby reducing the traits or variables that need be considered. PCA finds the axes of greatest variation in the dataset and reduces the number of variables viewed. This type of analysis is appropriate for statistical comparisons with smaller sample sizes where there are many variables and few specimens. In this way, data is simplified and it is easier to visualize and interpret the extent and distribution of variance.

Appendix B: Euclidean Distance Matrix Analysis (EDMA) Supplement

Reference (Lele and Richtsmeier 2001)

Throughout the discussion of EDMA, form refers to representations that include aspects of size and shape of the object. Shape refers to a 'size-corrected' form in which a scaling factor has been applied to investigate the differences that can be overwhelmed when scale is included.

EDMA Basics

Landmark data was further analyzed using EDMA. This approach uses matrix algebra. A matrix is a rectangular arrangement of values (referred to as elements) that are organized into rows and columns. In the explanations that follow, i represents the rows and j represents the columns. The symbol, a, denotes an element in the matrix. Therefore, a_{ij} denotes the element in the i-th row and the j-th column.

To accomplish this analysis, the landmark coordinates were used to calculate all possible linear distances (Euclidean distances) between landmark pairs. A matrix consisting of these distances is known as the form matrix (FM) of the object. This matrix represents the object being examined and this representation does not change with any translation, rotation or reflection of the object; therefore, this approach eliminates the influence of these parameters on the results. The form matrix is square (the number of rows equals the number of columns) and it is symmetric (aij = aji).

The form matrix is a square, symmetric matrix where d_{ij} is the Euclidean distance between landmarks *i* and *j*. For example, the element, $d_{1,2}$ in the diagramed form matrix below for object X, indicates the distance between landmark 1 and landmark 2. Where K is the number of landmarks, the number of unique pair-wise linear distances in a form matrix is K (K-1)/2 (Lele and Richtsmeier 2001).

$$FM(X) = \begin{bmatrix} 0 & d_{1,2} & d_{1,3} & d_{1,4} & \ldots & d_{1,k} \\ d_{2,1} & 0 & d_{2,3} & d_{2,4} & \ldots & d_{2,k} \\ d_{3,1} & d_{3,2} & 0 & d_{3,4} & \ldots & d_{3,k} \end{bmatrix}$$

Because the matrix is symmetric, it can be abbreviated by collecting all elements above the diagonal and expressing them as a vector (a matrix that has only 1 column).

When comparing two objects, X and Y, their form matrices FM(X) and FM(Y) are compared and the difference between forms is expressed as a form difference matrix (FDM). Elements of the form difference matrix correspond to the ratios (division of an element in one form matrix by its corresponding element in the other form matrix) of the linear distances.

When comparing groups, the mean form must be estimated for each group. The mean form matrix can be thought of as the average of the linear distances from all forms in the sample. The mean form difference matrix represents the difference between the mean forms of each group.

To account for size differences, the geometric mean of all distances can be used as a scaling factor to create a shape matrix. The outcome is size-corrected forms that, when compared, are considered a comparison of shape. The mean shape difference matrix represents the shape difference between sample groups. The elements of the shape difference matrix correspond to the difference between like linear distances of the two shape matrices.

Appendix C: Permissions

Confirmation Number: 11348656
Order Date: 04/27/2015

Order Details

[Biochimica et biophysica acta. Biomembranes](#)

- **Order detail ID:** 66857472
- **ISSN:** 0005-2736
- **Publication Type:** Journal
- **Volume:**
- **Issue:**
- **Start page:**
- **Publisher:** ELSEVIER BV

- **Permission Status:** ✅ **Granted**
- **Permission type:** Republish or display content
- **Type of use:** Thesis/Dissertation

   Order License Id: 3617220628131

Curriculum Vitae

Name:	Deidre Caskenette

Post-secondary Education and Degrees:

University of Guelph
Guelph, Ontario, Canada
1994-1998 B.Sc.

The University of Western Ontario
London, Ontario, Canada
2013-2015 M.Sc.

Honours and Awards:

Western Graduate Scholarship
2013-2015

Poster Presentation Finalist
American Association of Anatomists
2015

Nominated for W.H. Boyd Scholarship
(Highest Grade in Human Anatomy)
1997

Related Work Experience

Teaching Assistantships

University of Western Ontario, London, Ontario

Human Gross Anatomy Teaching - Lab Component for First and Second Year Medical Students	**Jan 2015 – Apr 2015**
Head Teaching Assistant for Systemic Human Anatomy Online (ANATCELL 3319)	**Sept 2014 - Apr 2015**
Systemic Human Anatomy Online (ANATCELL 3319)	**May 2014 - Aug 2014**

Human Functional Anatomy   **Jan 2014 – Apr 2014**
for School of Nursing (HEALTSCI 2330B)

Teaching Assistant for Human Gross Functional Anatomy
for   School of Physiotherapy (ANATCELL 9501) /   **Sept 2013 – Mar 2014**
School of Occupational Therapy (ANATCELL 9524)

Guest Lectures
University of Western Ontario, London, Ontario

Guest Lecturer for Histology Pre-Lab Talk for Mammalian   **Apr 7, 2014**
Histology (ANATCELL 3309)

Guest Lecturer for Tutorial for Clinical Mammalian Histology Mar 3, 2014
(ANATCELL 9561)
University of Western Ontario, London, Ontario

Functional Anatomy for School of Nursing   **Feb 27,2015**
(HEALTSCI 2330B 001)
University of Western Ontario, London, Ontario

PRESENTATIONS

•Caskenette, D., Laird, D.W., Wilson, T., Merrifield,P., Penuela, S., Willmore, K. (2014, October) Phenotypic Analysis of Long Bones in Pannexin 3 Knockout Mice Using a Geometric Morphometric Approach. Poster Presented at the Western Anatomy and Cell Biology Research Day, London, Ontario.

•Caskenette, D., Laird, D.W., Wilson, T., Merrifield,P., Penuela, S., Willmore, K. (2014, October) Phenotypic Analysis of Long Bones in Pannexin 3 Knockout Mice Using a Geometric Morphometric Approach. Poster Presented at Experimental Biology Symposium 2015, Boston, Massachusetts.

•Invited Platform Presentation (2015, March) Phenotypic Analysis of Long Bones in Pannexin 3 Knockout Mice Using a Geometric Morphometric Approach. Talk presented at Nexin Forum, London, Ontario.

VOLUNTEER EXPERIENCE

Foot Clinic Volunteer   **Sept 26, 2014**
University of Western Ontario, London, Ontario

- Assisted with dissections of foot and lower limb and acted
  as a resource in a workshop for foot care practitioners.

Let's Talk Science Graduate Student Volunteer   **Sept 2013 – Jun 2014**
University of Western Ontario, London, Ontario

- Performed demonstrations illustrating scientific principles
  and interacted with elementary school students
  participating in activities designed to educate and inspire
  children regarding scientific discovery.